Biomaterials Advances 154 (2023) 213649

Contents lists available at ScienceDirect

Biomaterials Advances

journal homepage: www.journals.elsevier.com/materials-science-and-engineering-c

Design of PLGA nanoparticles for sustained release of hydroxyl-FK866 by microfluidics

Xue Bai [a,1], Siyuan Tang [a,2], Sam Butterworth [a], Annalisa Tirella [a,b,*]

[a] Division of Pharmacy and Optometry, School of Health Science, Faculty of Biology, Medicine and Health, University of Manchester, Oxford Road, Manchester M13 9PT, UK

[b] BIOtech Center for Biomedical Technologies, Department of Industrial Engineering, University of Trento, Via delle Regole 101, 38123 Trento, Italy

ARTICLE INFO

Keywords:
PLGA
Nanoparticles
Hydroxyl-FK866
Drug-polymer conjugate
Microfluidics
Sustained drug release systems

ABSTRACT

The use of nanoparticle (NP) delivery systems in cancer treatment has received significant interest, however use of such systems in delivery of cytotoxic chemotherapy agents can be limited by low encapsulation efficiency and burst release of the cytotoxin, as well issues with throughput and reproducibility during the fabrication of drug-loaded NPs. In this study, we used a hydrodynamic flow-focusing microfluidic system to successfully produce poly(lactic-*co*-glycolic acid) (PLGA) NPs. The physico-chemical properties of PLGA NPs were controlled by changing the manufacturing parameters, such as flow rate ratio, total flow rate, PLGA and surfactant concentration. The NAMPT inhibitor-polymer conjugate, hydroxyl-FK866-PLGA, was synthesized and used to fabricate hydroxyl-FK866-PLGA NPs for the formulation of localized delivery systems able to release low doses of cytotoxins and enhance the efficacy of NAMPT inhibitors. Hydroxyl-FK866-PLGA NPs were prepared with optimized fabrication parameters, having average Z-size of 128 ± 8 nm (PDI < 0.2), ζ-potential of −14.8 ± 5.3 mV and high encapsulation efficiency (98.6 ± 5.8 %). The pH-dependent release of hydroxyl-FK866 was monitored over time in conditions mimicking the normal (pH 7.4) and inflamed/tumor (pH 6.4) microenvironments, observing a sustained release pattern (over two months) without any initial burst release. Finally, toxicity of hydroxyl-FK866-PLGA NPs were tested in selected human cell lines, the human leukemia monocytic cell line (THP-1), and the human triple negative breast cancer cell line (MDA-MB-231). Our work suggests that microfluidic systems are a promising technology for a rapid and efficient manufacturing of PLGA-based NPs for the controlled release of cytotoxins. Moreover, the use of drug-polymer conjugates is an effective approach for the manufacturing of polymeric NPs enabling high encapsulation efficiency and a prolonged and sustained pH-dependent drug release.

1. Introduction

Cancer kills around 10 million people in the world every year [1]. Cytotoxic chemotherapy, one of the most commonly used cancer treatments, can prolong the lives of patients; however, it often causes serious side effects, such as gastric irritation and marrow suppression [2]. Since their discovery, nanoparticles (NPs) have been used as drug delivery system (DDS), often used for the treatment of many diseases such as cancer. Liposomes, dendrimers, micelles and polymeric NPs are examples of commonly used nanoparticles to load therapeutic agents for cancer treatment [3]. Over the past years, nanoparticles have been progressively modified to improve their performances and with the scope to 1) enhance specificity towards cancerous cells, 2) reduce toxic effects to normal cells, 3) enable imaging of cancerous masses and 4) respond to external stimuli.

Polymeric NPs have been seen as promising DDS, with specific reference to reach a target tissue and overall improve bioavailability. These are formulated using several natural and/or synthetic polymers, such as polyethylene glycol (PEG), chitosan, poly (lactic acid) (PLA), poly (lactic-co-glycolic acid) (PLGA) and block-copolymers [3]. Among these, PLGA, a copolymer of PLA and poly glycolic acid (PGA), is one of the most commonly used synthetic polymers for the fabrication of

* Corresponding author at: Division of Pharmacy and Optometry, School of Health Science, Faculty of Biology, Medicine and Health, University of Manchester, Oxford Road, Manchester M13 9PT, UK.

E-mail addresses: annalisa.tirella@manchester.ac.uk, annalisa.tirella@unitn.it (A. Tirella).

[1] Present address: Institute of Food Science and Technology, Chinese Academy of Agricultural Sciences/Key Laboratory of Agro-Products Processing, Ministry of Agriculture, Beijing 100193, China.

[2] Present address: School of Physical Science and Technology, ShanghaiTech University, 201210, Shanghai, China.

https://doi.org/10.1016/j.bioadv.2023.213649
Received 13 February 2023; Received in revised form 25 September 2023; Accepted 30 September 2023
Available online 4 October 2023

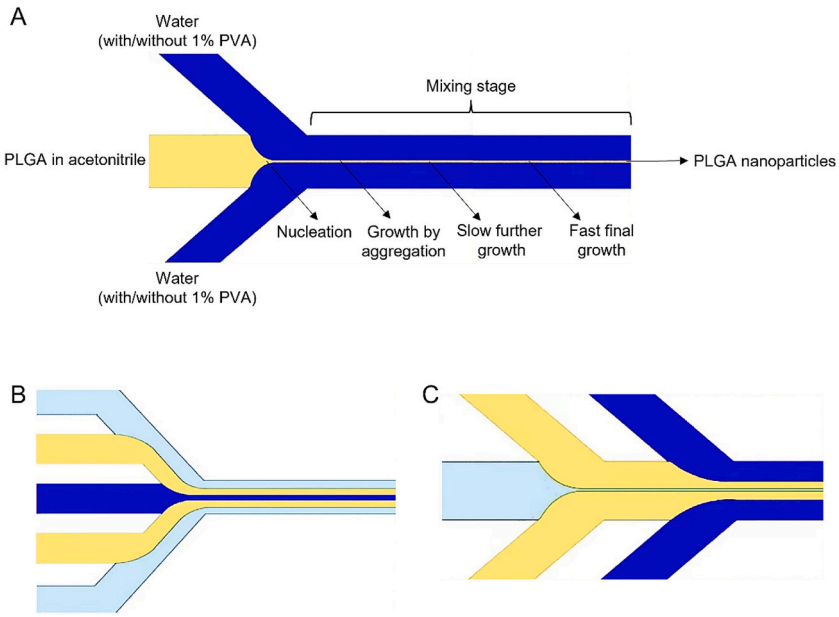

Fig. 1. Hydrodynamic focusing designs of continuous microfluidic chips: A) Schematic illustration used for PLGA NPs production by the hydrodynamic flow focusing; B) hydrodynamic focusing design with additional sheath-flows to improve flow stability; C) multiple hydrodynamic focusing steps.

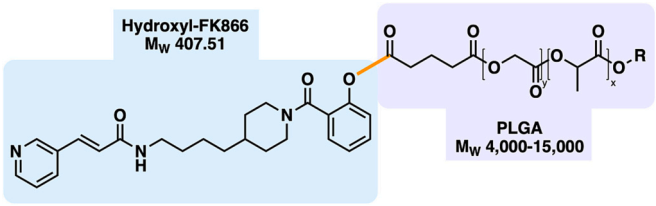

Fig. 2. Structures of hydroxyl-FK866-PLGA conjugate (light blue rectangle: hydroxyl-FK866; purple rectangle: PLGA; phenolic ester bond and cleavable site: orange).

polymeric NPs. PLGA is FDA approved and has been used for decades in many clinical applications thanks to its biodegradability, biocompatibility and non-toxicity [4]. PLGA NPs can be prepared in different sizes and formulations, and using many fabrication methods, such as water-in-oil (w/o) phase separation, water-in-oil-in-water (w1/o/w2) emulsion and spray drying [4]. Over the past decades, microfluidics has been proposed as emerging technology for the manufacturing of polymeric NPs, including PLGA [3,5]. Microfluidics enable a precise control of the flow of small volumes of fluids (10^{-18} to 10^{-9} L) over channels with different geometries and sizes (10^{-6} to 10^{-4} m), and it is widely used to control the mixing of two or more components [6]. When it comes to the preparation of NPs, and when compared to batch preparation methods, microfluidics provide many benefits including generation of monodisperse and uniform droplet emulsions, use of small amounts of solvents and materials, better control of processing parameters overall reduced manufacturing time and associated costs, and easy scale-up production [7,8]. Moreover, depending on the chip geometry, microchannels size and flow configuration, microfluidic systems are classified in two categories: droplet-based (or segmented flow) and continuous flow microfluidics [9]. Sub-categories of droplet-based geometries, based on how the flow of two phases are inter/connected, are co-flow, cross-flow, and flow-focusing [10]. Continuous phase flow microfluidics is designed to have two or more fluids flowing side-by-side in microchannels without segmentation. When two immiscible fluids mix within the channel, a shortened mixing time could lead to the formation of NPs. The most common configurations used for the fabrication of NPs using continuous phase flow microfluidic systems are represented in Fig. 1 [9]. In this work, a hydrodynamic flow-focusing chip and a temperature-controlled microfluidic system was used to control the flow of the organic (PLGA in acetonitrile) and aqueous (PVA in water) phases; where the latter was used as the anti-solvent to trigger PLGA particle nucleation, growth and precipitation (Fig. 1A). In specific, the central organic phase is constrained to flow into a narrow stream between the two aqueous phases (flow focus), which enable the mixing of the two immiscible solutions through diffusion [11]. Because of the high solubility of PLGA in acetonitrile and its low solubility in water, during mixing PLGA precipitates as particles/aggregates [12]. The microfluidic system it also allows to precisely control, and fluid distribution inside the channel (hence prevents particle formation close to the channel walls and reducing channel clogging) [9].

In this study, the following manufacturing parameters were selected to investigate their role on the characteristics of fabricated NPs: flow rate ratio (flow rate of organic phase to aqueous phase, FRR), total flow rate (TFR), PLGA concentration in acetonitrile (organic phase), and presence of poly(vinyl) alcohol (PVA) as surfactant (aqueous phase). PVA, a hydrophilic and biocompatible polymer widely used as synthetic water-soluble polymer surfactant, with excellent chemical and physical properties, easy processing and low cytotoxicity [13].

As the X-ray crystal structure showing a solvent-exposed region of the molecule suitable for modification, in this study, FK866 was designed and conjugated to PLGA via hydrolytically cleavable linkage (Fig. 2) with the aim of achieving a prolonged and sustained release in the acidic inflamed/cancerous environment (approx. pH value of 6.5) [14].

FK866, a cytotoxic compound, is a highly potent and specific inhibitor of the biosynthesis of the coenzyme nicotinamide adenine dinucleotide, thereby causing irreversible cell death induced by apoptosis and FK866 has been shown to regulate all three stages of the apoptotic cascade in-vitro [15]. Clinical development of FK866 was discontinued due to poor efficacy at tolerated doses, which were limited by side effects including thrombocytopenia, linked to poor tumor specificity [15]. These findings suggest that future development of NAMPT inhibitors will require localized or targeted delivery to the tumor microenvironment, resulting in several large pharmaceutical companies utilizing distinct series of NAMPT inhibitors as novel payloads for antibody-drug conjugates [16,17]. Due to the high potency of

FK866 and the availability of an X-ray crystal structure showing a solvent-exposed region of the molecule suitable for modification, this compound was selected for this study and conjugated to PLGA via hydrolytically cleavable linkage (Fig. 2) with the aim of achieving a prolonged and sustained release in the acidic inflamed/cancerous environment (approx. pH value of 6.5) [14].

The formulation of the drug-PLGA conjugate as NPs can address the drawbacks of drug-loaded NPs, such as low encapsulation efficiency (EE) and initial drug burst release; typically hindering the translation of PLGA NPs into clinical applications. This design could be advanced with specific functionalization of NPs surface and use as injectable systems able to be retained in-situ and release the loaded drug at the injection site (e.g., peri-tumoral, intra-tumoral). This approach advances beyond the traditional formulation of NPs for oral [18], nasal [19] or intravenous delivery [20]; and uses other routes of administration to address reported clinical issues such as off-target accumulation and delivery or required dose at the site of intervention, increasing efficacy and reducing damage to healthy tissues.

2. Materials and methods

2.1. Materials

Poly(lactic-*co*-glycolic acid) (PLGA, RG752H, Product No. 719919, lactide:glycolide 75:25, Mw 4000–15,000) and PLGA (RG502H, Product No. 719897, lactide:glycolide 50:50, Mw 7000–17,000) were purchased from Resomer (Sigma Aldrich, UK). Poly (vinyl alcohol) (PVA, Product No. 360627-25G), citric acid (Product No. 251275), Dulbecco's Modified Eagle's medium (DMEM, D6429), RPMI-1640 medium (R0883), fetal bovine serum (FBS, F9665), trypsin (T3924), L-glutamine (G7513), antibiotics (penicillin − streptomycin, P0781), trypan blue (Product No. 15250061), cell proliferation reagent WST-1 (Product No. CELLPRO-RO), 4′,6-Diamidino-2-Phenylindole (DAPI, D9542), 4 % formaldehyde solution (pH 6.4, buffered, 1,004,968,350) were purchased from Sigma-Aldrich (UK). HPLC-grade water (H_20, 389,390,025), tris base (BP152–1), hydrochloric acid (HCl, 12,666,846) and sodium hydrogen phosphate (Na_2HPO_4, 11,438,970) were purchased from Fisher Scientific (UK). Acetonitrile (HPLC-grade, 34,851–2.5 L) and methanol (HPLC-grade, 34,966–2.5 L) were purchased from Honeywell.

2.2. Synthesis of hydroxyl-FK866-PLGA and model compounds

2.2.1. General information

Commercial reagents and solvents were used directly without further purification. Anhydrous solvents were supplied by Acros Organics over 4 Å molecular sieves. Glassware such as round bottom flasks and ace pressure tubes were dried in the oven first and then heated with a heating gun under vacuum. Progress of the reaction was monitored with TLC using F_{245} aluminium-backed silica gel plate purchased from Merck. UV light (254/365 nm) and $KMnO_4$ were used for visualization. The following cooling baths were used: 0 °C (ice/water), −10 °C (ice/MeOH), −40 °C (dry ice/MeCN) and −78 °C (dry ice/acetone). For heating reactions, paraffin oil baths and stirrer hotplates were used, and the temperature was monitored using a thermometer. Compounds were purified by flash column chromatography (silica gel) using Geduran silica gel 60 or reverse phase flash column chromatography CombiFlash® machine using 5.5 g, 15.5 g or 30.0 g C18 Gold columns with 20–40 μm silica, eluting with a gradient 0 % to 100 % MeCN in water as acid method (0.1 % formic acid as modifier) or base method (0.1 % NH_4OH as modifier) as indicated, or by prep HPLC using C18 Kinetex HPLC column with 5 μm silica, eluting with a gradient 0 % to 100 % MeCN in water.

2.2.1.1. NMR. NMR spectra were recorded on a Bruker AV400 (^1H = 400 MHz, ^{13}C = 101 MHz) spectrometer in commercial deuterated solvents. Chemical shift (δ) were reported in ppm and spectra were recorded in $CDCl_3$ referenced to residual $CHCl_3$ (δ_H 7.26 ppm, δ_C 77.16 ppm), CD_3OD referenced to residual MeOH (δ_H 3.31 ppm, δ_C 49.00 ppm) or $(CD_3)_2SO$ referenced to residual DMSO (δ_H 2.50 ppm, δ_C 39.52 ppm). Coupling constants *J* were reported in Hz to the nearest 0.1 Hz. Coupling constants that were non-identical were reported as averages. Data were processed on Mestrenova 14.0.1. Unless stated otherwise, ^{31}P were reported decoupled to ^1H, ^{19}F were reported coupled to ^1H. All ^1H and ^{13}C assignments were supported by two-dimensional spectrum ^1H—^1H COSY, ^1H—^1H NOESY, ^1H—^{13}C HSQC and ^1H—^{13}C HMBC.

2.2.1.2. MS. Mass spectra were recorded on Waters ACQUITY QDa detector.

2.2.2. Experimental procedures and analytical data

2-(Piperidine-1-carbonyl)phenyl acetate (1) 2-Acetoxybenzoic acid (180 mg, 1 mmol) was dissolved in anhydrous DMF (10 mL). Piperidine (0.10 mL, 1 mmol), HATU (570 mg, 1.50 mmol) and DIPEA (0.35 mL, 2.00 mmol) were added under argon atmosphere. The mixture was stirred overnight under argon atmosphere at RT. The reaction mixture was quenched with water (40 mL) and extracted with EtOAc (3 × 20 mL). The organic phases were combined, dried over $MgSO_4$, filtered, and concentrated under reduced pressure to provide a yellow oil. The crude material was purified by CombiFlash® using acid method to afford the title compound as a colourless oil. **Yield**: 182 mg, 0.74 mmol, 74 %. **^{1}H NMR** (400 MHz, $CDCl_3$) δ_H 7.37 (ddd, *J* = 8.2, 7.0, 2.1 Hz, 1H), 7.30–7.19 (m, 2H), 7.13 (dd, *J* = 8.1, 1.1 Hz, 1H), 3.67 (s, 2H), 3.20 (t, *J* = 5.5 Hz, 2H), 2.25 (s, 3H), 1.62 (s, 4H), 1.47 (q, *J* = 5.3 Hz, 2H). **^{13}C NMR** (101 MHz, $CDCl_3$) δ_C 169.10, 166.46, 147.00, 147.00, 130.05, 127.61, 126.06, 123.04, 48.34, 42.74, 26.39, 25.81, 24.58, 21.05. **MS** *m/z* (ES^+) 248.4 $[M + H]^+$.

3-(Piperidine-1-carbonyl)phenyl acetate (2) 3-Acetoxybenzoic acid (180 mg, 1 mmol) was dissolved in anhydrous DMF (10 mL). Piperidine (0.10 mL, 1 mmol), HATU (570 mg, 1.50 mmol) and DIPEA (0.35 mL, 2.00 mmol) were added under argon atmosphere. The mixture was stirred overnight under argon atmosphere at RT. The reaction mixture was quenched with water (40 mL) and extracted with EtOAc (3 × 20 mL). The organic phases were combined, dried over $MgSO_4$, filtered, and concentrated under reduced pressure to provide a yellow oil. The crude material was purified by CombiFlash® using acid method to afford the title compound as a colourless oil. **Yield**: 164 mg, 0.66 mmol, 66 %. **^{1}H NMR** (400 MHz, $CDCl_3$) δ_H 7.40–7.27 (m, 1H), 7.18 (dt, *J* = 7.7, 1.4 Hz, 1H), 7.06 (dddd, *J* = 4.8, 3.5, 2.4, 1.1 Hz, 2H), 3.62 (s, 2H), 3.29 (s, 2H), 2.23 (s, 3H), 1.69–1.39 (m, 6H). **^{13}C NMR** (101 MHz, $CDCl_3$) δ_C 169.05, 150.49, 137.76, 129.55, 124.22, 122.59, 120.31, 48.78, 43.21, 26.51, 25.62, 24.55, 21.14. **MS** *m/z* (ES^+) 248.4 $[M + H]^+$.

Benzyl but-3-yn-1-ylcarbamate (4) But-3-yn-1-amine hydrochloride (**3**, 1000 mg, 9.52 mmol) was dissolved in anhydrous DCM (40 mL). Benzyl chloroformate (3.80 mL from a 3 M THF solution, 11.40 mmol) and TEA (3.96 mL, 28.56 mmol) were added under argon atmosphere. The mixture was stirred for 1 h under argon atmosphere at 0 °C. The reaction mixture was quenched with water (80 mL) and extracted with EtOAc (3 × 40 mL). The organic phases were combined, dried over $MgSO_4$, filtered, and concentrated under reduced pressure to provide a colourless oil. The crude material was purified by CombiFlash® using base method to afford the title compound as a colourless oil. **Yield**: 649 mg, 3.20 mmol, 34 %. **^{1}H NMR** (400 MHz, $CDCl_3$) δ_H 7.41–7.27 (m, 5H), 5.11 (s, 2H), 3.36 (q, *J* = 6.4 Hz, 2H), 2.41 (td, *J* = 6.5, 2.7 Hz, 2H), 2.00 (t, *J* = 2.6 Hz, 1H), 1.64 (s, 1H). **^{13}C NMR** (101 MHz, $CDCl_3$) δ_C 156.35, 136.54, 128.68, 128.31, 128.28, 81.50, 70.22, 66.95, 39.82, 20.02.

***tert*-Butyl 4-(4-(((benzyloxy)carbonyl)amino)but-1-yn-1-yl)-3,6-dihydropyridine-1(2*H*)-carboxylate (5)** *tert*-Butyl 4-bromo-3,6-dihydropyridine-1(2*H*)-carboxylate (129 mg, 0.49 mmol) was dissolved in anhydrous DMF (6 mL). **4** (100 mg, 0.49 mmol), $PdCl_2(PPh_3)_2$ (17 mg, 0.02 mmol), CuI (2 mg, 0.01 mmol) and TEA (1.37 mL, 9.84 mmol) were

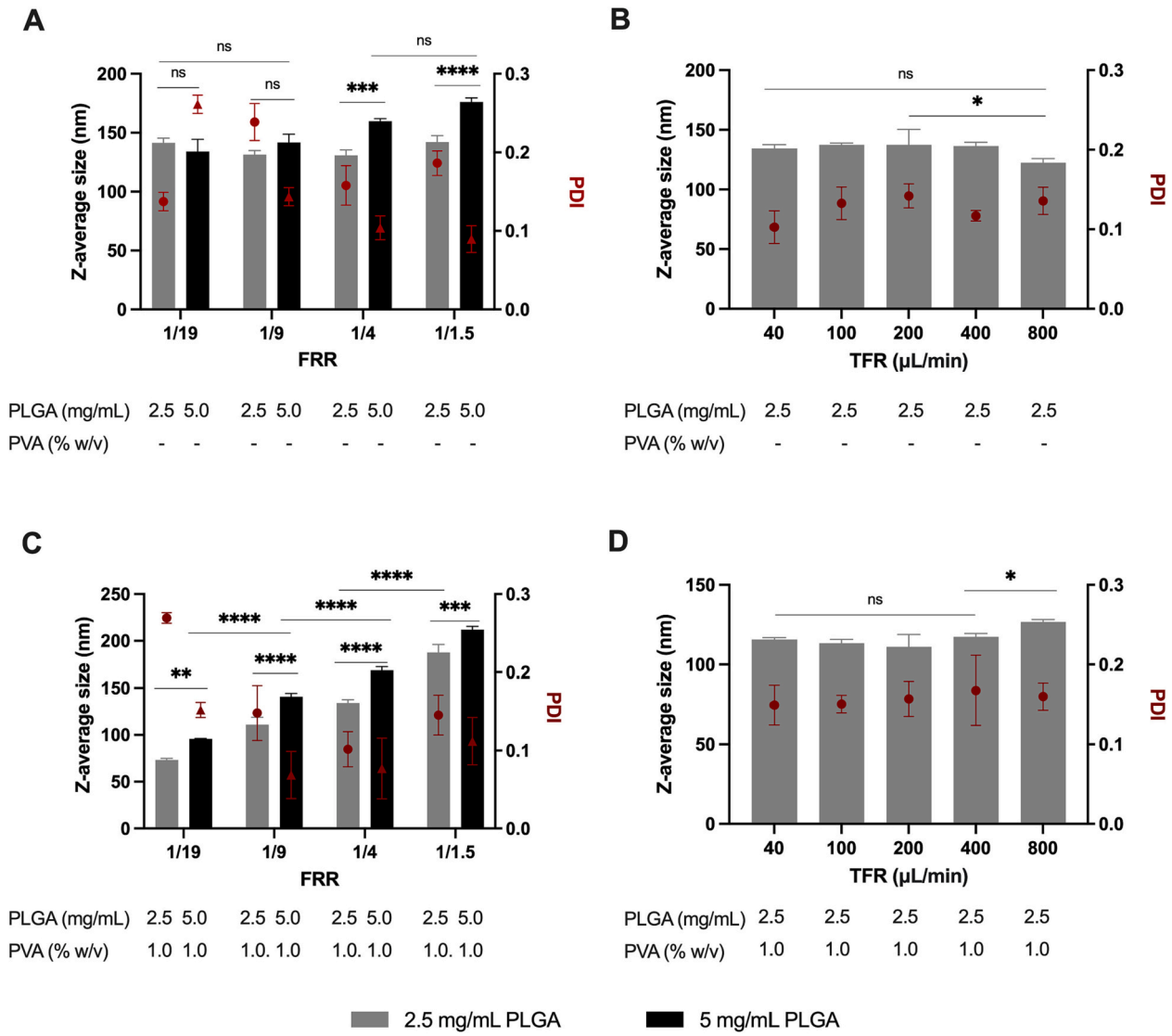

Fig. 3. PLGA nanoparticles Z-average size: effect of FRR, TFR, PLGA concentration (2.5 mg/mL and 5.0 mg/mL, respectively plotted in grey and black) and surfactant (1 % w/v PVA) as follows: A) TFR = 200 μL/min and pure water as the aqueous phase; B) FRR = 1/9 and pure water as the aqueous phase; C) TFR = 200 μL/min and 1 % w/v PVA (aq.) as the aqueous phase; D) FRR = 1/9 FRR and 1 % w/v PVA (aq.) as the aqueous phase. Temperature was set as 25 °C when preparing all the NPs. Z-average size and PDI were measured by dynamic light scattering (DLS), data is presented as average ± st.dev. ($N = 3$ independent experiments). Differences were considered significant at $p < 0.05$ (*$p \leq 0.05$, **$p \leq 0.01$, ***$p \leq 0.001$, ****$p \leq 0.0001$).

added under argon atmosphere. The mixture was stirred overnight under argon atmosphere at 80 °C. The reaction mixture was quenched with water (30 mL) and extracted with EtOAc (3 × 20 mL). The organic phases were combined, dried over $MgSO_4$, filtered, and concentrated under reduced pressure to provide a brown oil. The crude material was purified by flash column chromatography (silica gel), eluting with 1 % MeOH in DCM to afford the title compound as a colourless oil. **Yield**: 83 mg, 0.22 mmol, 45 %. **^{1}H NMR** (400 MHz, $CDCl_3$) δ_H 7.41–7.27 (m, 5H), 5.92 (s, 1H), 5.08 (d, $J = 20.6$ Hz, 3H), 3.93 (q, $J = 3.0$ Hz, 2H), 3.47 (t, $J = 5.7$ Hz, 2H), 3.35 (q, $J = 6.4$ Hz, 2H), 2.52 (t, $J = 6.5$ Hz, 2H), 2.18 (s, 2H), 1.46 (s, 9H). **^{13}C NMR** (101 MHz, $CDCl_3$) δ_C 156.35, 154.86, 136.56, 128.68, 128.32, 119.43, 85.94, 82.36, 79.96, 66.94, 43.76, 40.10, 29.57, 28.57, 20.88. **MS** *m/z* (ES^+) 285.3 $[M\text{-Boc}]^+$.

***tert*-Butyl 4-(4-aminobutyl)piperidine-1-carboxylate (6) 5** (68 mg, 0.18 mmol) was dissolved in a mixture of DCM and MeOH (10 + 10 mL). Pd/C (10 mg, 10 % Pd) was added under argon atmosphere. The mixture was stirred for 2 h under hydrogen atmosphere. The Pd/C was filtered off through a pad of Celite® and the organic solution was concentrated under reduced pressure to afford the title compound as a colourless oil without any further purification.

***tert*-Butyl (*E*)-4-(4-(3-(pyridin-3-yl)acrylamido)butyl)piperidine-1-carboxylate (7) 6** (0.18 mmol as hypothetic quantitative yield from last step) was dissolved in anhydrous DMF (10 mL). (*E*)-3-(Pyridin-3-yl)acrylic acid (32 mg, 0.21 mmol), HATU (101 mg, 0.27 mmol) and DIPEA (0.06 mL, 0.35 mmol) were added under argon atmosphere. The mixture was stirred overnight under argon atmosphere at RT. The reaction mixture was quenched with water (40 mL) and extracted with EtOAc (3 × 20 mL). The organic phases were combined, dried over $MgSO_4$, filtered, and concentrated under reduced pressure to provide a yellow oil. The crude material was purified by CombiFlash® using base method to afford the title compound as a colourless oil. **Yield**: 40 mg, 0.11 mmol, 61 % over 2-steps. **^{1}H NMR** (400 MHz, $CDCl_3$) δ_H 8.60 (s, 1H), 8.42 (d, $J = 4.7$ Hz, 1H), 7.66 (dt, $J = 8.0$, 1.9 Hz, 1H), 7.49 (d, $J = 15.7$ Hz, 1H), 7.17 (dd, $J = 8.0$, 4.8 Hz, 1H), 7.07 (t, $J = 5.8$ Hz, 1H), 6.55 (d, $J = 15.7$ Hz, 1H), 3.96 (t, $J = 9.1$ Hz, 2H), 3.27 (q, $J = 6.8$ Hz, 2H), 2.54 (t, $J = 13.0$ Hz, 2H), 1.55–1.42 (m, 4H), 1.35 (s, 9H), 1.30–1.04 (m, 5H), 0.92 (qd, $J = 12.2$, 4.3 Hz, 2H). **^{13}C NMR** (101 MHz, $CDCl_3$) δ_C 165.35, 154.82, 149.94, 148.85, 136.39, 134.25, 130.88,

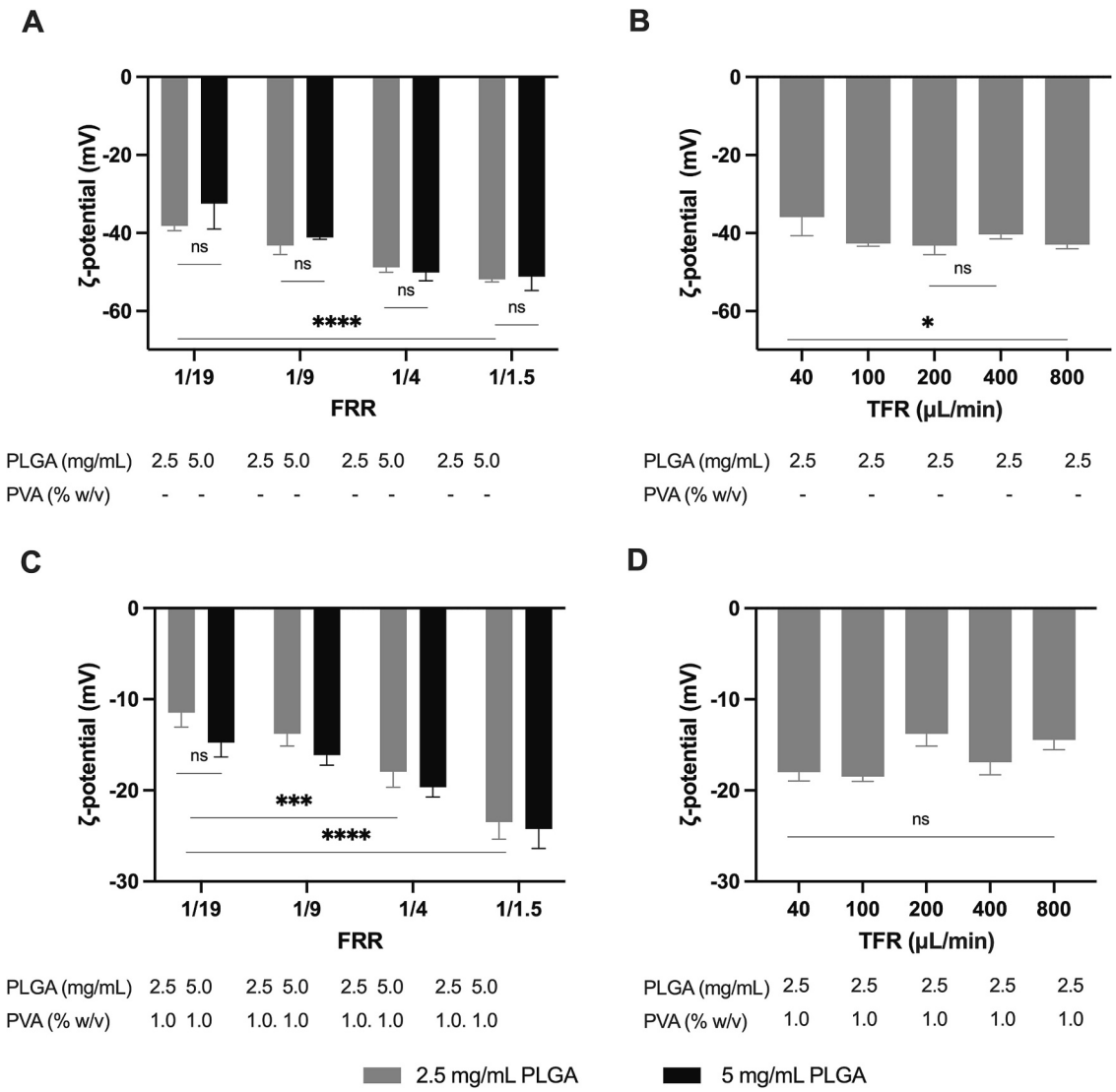

Fig. 4. ζ-Potential of PLGA NPs: effect of FRR, TFR, PLGA concentration (2.5 mg/mL and 5.0 mg/mL, respectively grey and black) and surfactant (1 % w/v PVA) as follows: A) TFR = 200 μL/min and pure water as the aqueous phase; B) FRR = 1/9 and pure water as the aqueous phase; C) TFR = 200 μL/min and 1 % w/v PVA (aq.) as the aqueous phase; D) FRR = 1/9 and 1 % w/v PVA (aq.) as the aqueous phase. Temperature was set as 25 °C when preparing all the nanoparticles. ζ-Potential was measured by dynamic light scattering (DLS), data is presented as average ± st.dev. ($N = 3$ independent experiments). Differences were considered significant at $p < 0.05$ (*$p \leq 0.05$, **$p \leq 0.01$, ***$p \leq 0.001$, ****$p \leq 0.0001$).

123.63, 123.52, 79.17, 43.94, 43.94, 39.66, 36.06, 35.74, 32.01, 29.71, 28.37, 23.93. **MS** *m/z* (ES^+) 288.8 $[M\text{-}Boc]^+$. **MS** *m/z* (ES^-) 386.4 $[M\text{-}H]^-$.

(*E*)-*N*-(4-(piperidin-4-yl)butyl)-3-(pyridin-3-yl)acrylamide (8) 7 (52 mg, 0.14 mmol) was dissolved in DCM (10 mL). HCl (1.68 mL from a 4 M water solution, 6.74 mmol) was added under argon atmosphere. The mixture was stirred for 4 h under argon atmosphere at RT. The reaction mixture was concentrated under reduced pressure to afford the title compound as a colourless oil without any further purification. **MS** *m/z* (ES^+) 288.4 $[M + H]^+$.

(*E*)-*N*-(4-(1-(2-hydroxybenzoyl)piperidin-4-yl)butyl)-3-(pyridin-3-yl)acrylamide (9) 8 (0.14 mmol as hypothetic quantitative yield from last step) was dissolved in anhydrous DMF (10 mL). 2-Hydroxybenzoic acid (19 mg, 0.14 mmol), HATU (77 mg, 0.20 mmol) and DIPEA (0.07 mL, 0.41 mmol) were added under argon atmosphere. The mixture was stirred overnight under argon atmosphere at RT. The reaction mixture was quenched with water (40 mL) and extracted with EtOAc (3 × 20 mL). The organic phases were combined, dried over $MgSO_4$, filtered, and concentrated under reduced pressure to provide a yellow oil. The crude material was purified by CombiFlash® using base method to afford the title compound as a colourless oil. **Yield**: 25 mg, 0.06 mmol, 43 % over 2-steps. **^{1}H NMR** (400 MHz, MeOD) δ_H 8.71 (s, 1H), 8.51 (d, $J = 4.8$ Hz, 1H), 8.03 (dt, $J = 8.1$, 1.9 Hz, 1H), 7.56 (s, 1H), 7.47 (dd, $J = 8.0$, 4.9 Hz, 1H), 7.24 (td, $J = 7.8$, 1.7 Hz, 1H), 7.13 (dd, $J = 7.5$, 1.7 Hz, 1H), 6.91–6.81 (m, 2H), 6.73 (d, $J = 15.8$ Hz, 1H), 3.31 (t, $J = 1.6$ Hz, 2H), 1.74 (s, 2H), 1.57 (p, $J = 7.1$ Hz, 3H), 1.41 (td, $J = 12.5$, 6.9 Hz, 2H), 1.37–1.28 (m, 2H), 1.26–1.19 (m, 1H), 1.19–1.11 (m, 2H). **^{13}C NMR** (101 MHz, MeOD) δ_C 170.51, 167.65, 154.98, 150.69, 149.65, 137.34, 136.25, 132.91, 131.72, 128.88, 125.55, 124.89, 124.83, 120.57, 116.73, 40.56, 37.15, 37.11, 33.45, 33.45, 33.45, 30.56, 25.04. **MS** *m/z* (ES^+) 408.5 $[M + H]^+$.

PLGA Polymer-OH-FK866 (10) 9 (25 mg, 0.06) was dissolved in anhydrous DCM (20 mL). PLGA Polymer (RG752H, 246 mg, 0.06 mmol), HATU (93 mg, 0.25 mmol) and DIPEA (0.09 mL, 0.49 mmol) were added under argon atmosphere. The mixture was stirred for 7 days under argon atmosphere at RT. The reaction mixture was concentrated under reduced pressure and MeOH was added (20 mL). The crude material was centrifuged, and the precipitated solid was washed with MeOH (2 × 20

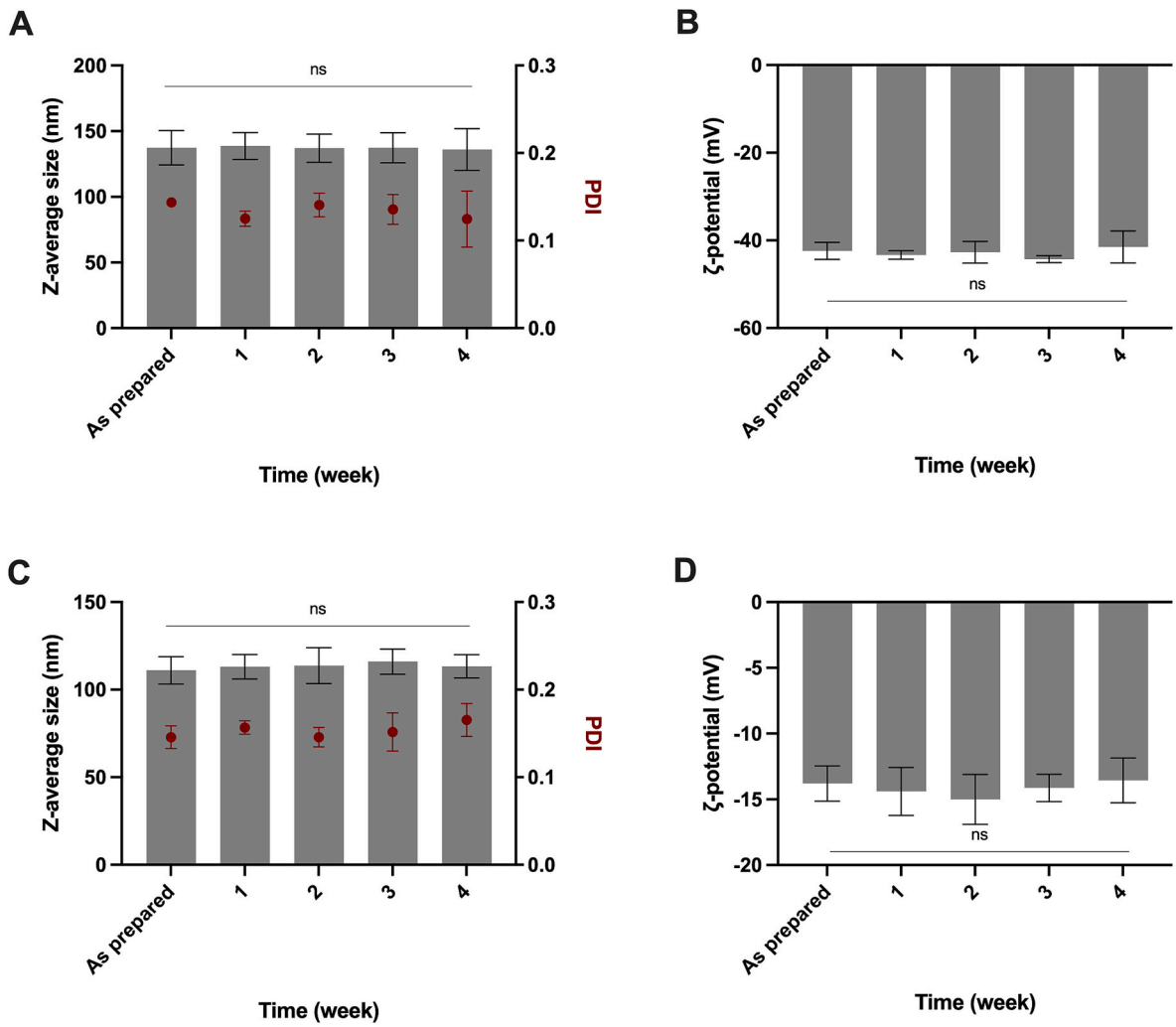

Fig. 5. Size and shape stability of drug-free PLGA NPs upon storage (4 °C, pH 7.4). PLGA NPs without 1 % w/v PVA (aq.): A) Z-average size and PDI, and B) ζ-potential; and PLGA NPs with 1 % w/v PVA (aq.): C) Z-average size and PDI, and D) ζ-potential. Manufacturing parameters: 2.5 mg/mL PLGA, FRR = 1/9, TFR = 200 μL/min, and temperature of 25 °C. Values were measured by dynamic light scattering (DLS), data is presented as average ± st.dev. (N = 3 independent experiments). Differences were considered significant at $p < 0.05$ (*$p \leq 0.05$, **$p \leq 0.01$, ***$p \leq 0.001$, ****$p \leq 0.0001$).

mL) and used without any further purification. **Yield:** 172 mg, 0.04 mmol, 67 %. **^{1}H NMR** (400 MHz, $CDCl_3$) δ_H 8.70 (d, J = 2.2 Hz, 1H), 8.52 (d, J = 4.8 Hz, 1H), 7.76 (d, J = 8.0 Hz, 1H), 7.56 (d, J = 15.5 Hz, 1H), 7.37 (s, 1H), 6.44 (d, J = 15.7 Hz, 1H), 5.15 (tdd, J = 19.1, 10.0, 5.0 Hz, 291H), 4.92–4.52 (m, 178H), 1.67–1.38 (m, 843H).

2.3. Nanoparticle preparation using microfluidic system

PLGA NPs were prepared using the automated Dolomite microfluidic system (Dolomite, Royston UK) equipped with the 5-input Chip (Part No. 3200735), Compressor (Part No. 3200117); Mitos P-Pump (Part No. 3200016); Mitos P-Pump Remote Chamber 30 (Part No. 3200178); Mitos Flow Rate Sensor 1–50 μL/min (Part No. 3200098); Mito Flow Rate Sensor 30–1000 μL/min (Part No. 3200097); Meros Temperature Control Unite (Part No. 3200428); In-line Valve (Part No. 3200087); T-Connector (Part No. 3000397).

The organic (or dispersed) phases were prepared using PLGA (RG752H, lactide:glycolide 75:25, Mw 4000–15,000), unless otherwise described, in acetonitrile at concentration of 2.5 mg/mL or 5.0 mg/mL, and hydroxyl-FK866-PLGA/rhodamine-PLGA in acetonitrile (both prepared with PLGA RG752H) at a concentration of 2.5 mg/mL. Pure HPLC-grade H_2O and a 1 % (w/v) PVA solution (aq.) were used as aqueous (or continuous) phase in all the experiments. Both aqueous and organic solutions were filtered twice through a 0.22 μm PVDF filters (Millex-CV, Merck Millipore Ltd. Germany) and 0.2 μm PTFE filters (code 1514–1499, Fisherbrand) separately prior each experiment. The temperature of solutions and chip were set and maintained at a temperature of 25 °C and a back pressure of 2 bars.

2.4. Physico-chemical characterization of nanoparticles

2.4.1. Dynamic light scattering (DLS)

NPs hydrodynamic diameter (Z-average size) and ζ-potential were measured at 50 μg/mL, 25 °C (pre-equilibration for 2 min) using a Zetasizer Nano ZS (model ZEN3600, Malvern Instruments Ltd., UK) equipped with a solid state HeNe laser (λ = 633 nm) at a scattering angle of 173°. Size distributions were calculated by applying the general-purpose algorithm and are presented as the average of the Z-average values of three (n = 3) independent samples.

2.4.2. Transmission electron microscopy (TEM)

A volume of 3 μL of each nanoparticle formulation was fixed on glow discharged (25 mA, 1 min) carbon film mesh copper grids using 50 μL of aqueous solution containing 2 % (v/v) uranyl acetate stain (negative staining) for 5 min. Grids were left to dry prior to analysis. Images ($n \geq 3$ of each preparation) were acquired using a transmission electron

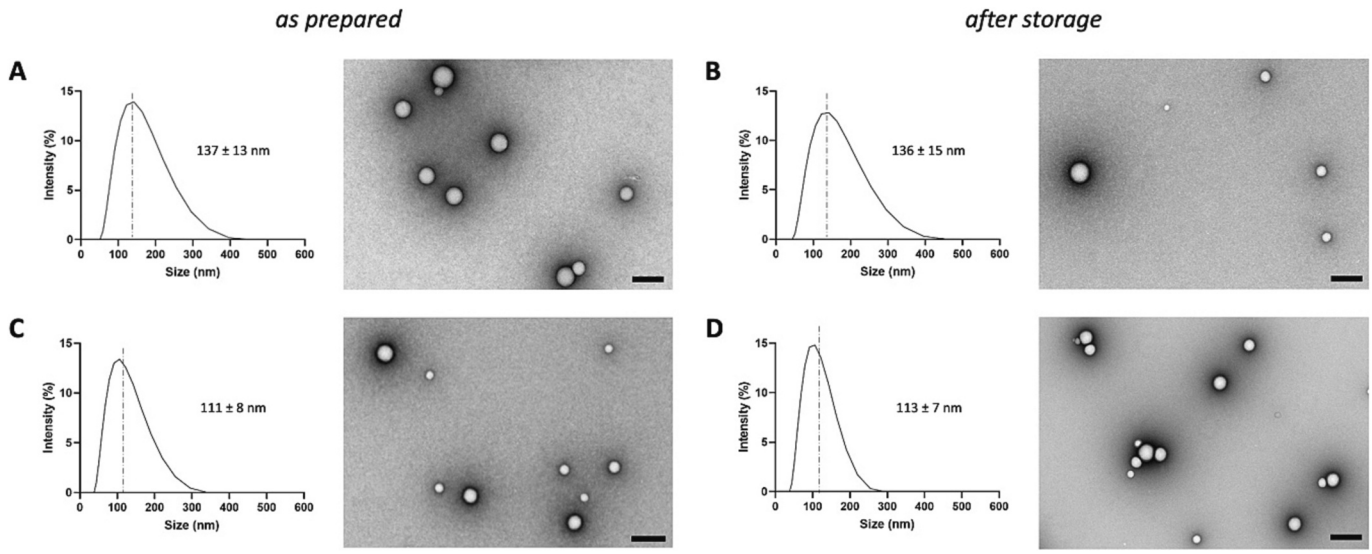

Fig. 6. Size and shape stability of PLGA NPs: examples of size distribution (DLS) and images (TEM) of PLGA NPs as prepared and after storage (4 weeks, 4 °C, pH 7.4): A) PLGA NPs as prepared; B) PLGA NPs after storage; C) PLGA NPs with PVA as prepared and D) PLGA NPs with PVA after storage. Manufacturing parameters: 2.5 mg/mL PLGA, 1 % w/v PVA (aq.), FRR = 1/9, TFR = 200 μL/min, and temperature of 25 °C. Scale bars: 200 nm.

Scheme 1. Synthesis of compound **1** and **2**.

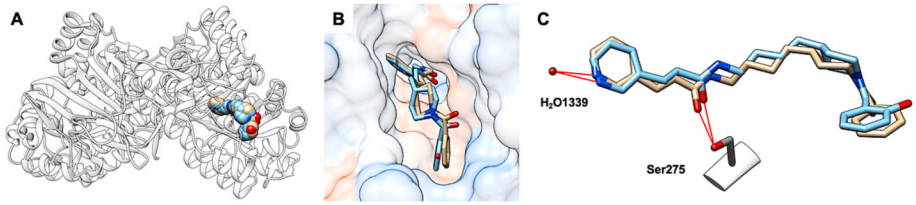

Fig. 7. Crystal structure of FK866 (in cream) bound to NAMPT (PDB entry: 2GVJ) and putative binding mode of hydroxyl-FK866 (in cyan) bound to NAMPT. A) FK866 (in cream sphere) and Hydroxy-FK866 (in cyan sphere) occupy identical binding site; B) FK866 (in cream stick) and hydroxyl-FK866 (in cyan stick) possess a similar orientation in the binding pocket. The binding pocket is generated and coloured by software UCSF Chimera 1.13.1 (orange = lipophilic, blue = hydrophilic); C) Both FK866 (in cream stick) and hydroxyl-FK866 (in cyan stick) illustrated identical hydrogen bonds (in red lines) towards Ser255 and H_2O 133 (Hydrogen bonds predicted by software UCSF Chimera 1.13.1).

microscope (FEI Tecnai 12 BioTwin) operated at an accelerating voltage of 100 kV.

2.4.3. *Drug loading, encapsulation efficiency and drug release*

A Perkin Elmer Series 200 HPLC system equipped with a C18 reverse-phased column (ACE™, 5 μm particle size, 150 × 4.6 mm i.d., Hichrom Ltd., Berkshire, UK) was used to quantify the amount of hydroxyl-FK866, both loaded in NPs formulations and released. Samples were eluted using 15 min isocratic system of acetonitrile (100 %, 0.1 % v/v TFA), and ultrapure distilled water (100 %, 0.1 % v/v TFA) with ratio, flow rate, injection volume and detection wavelength set at 30:70, 1 mL/min, 50 μL, and 257 nm respectively. The hydroxyl-FK866 peak was detected at 3.6 min. Hydroxyl-FK866 stock solutions in the concentration range of 0.05–5 μg/mL were diluted in pure water and used to obtain a linear calibration curve.

2.4.3.1. Drug loading. Drug loading was calculated based on the ^{1}H NMR analysis. For the NMR analysis, ratios were determined for the peak integrals representing aromatic protons (hydroxyl-FK866), the methine protons (lactic acid) and methylene protons (glycolic acid). The drug loading was calculated by the ratio of multiplying the corresponding protons' peak area by the molecular weight ratio of each component.

2.4.3.2. Encapsulation efficiency. The encapsulation efficiency (EE, Eq. (1)) was expressed as the percentage ratio of amount of drug encapsulated and total drug added. In this study, NPs were dialyzed (Float-A-Lyzer G2, MWCO: 0.5–1 kDa, SpectrumLabs) against milliQ water overnight at 4 °C to remove the potential free hydroxyl-FK866, and then the freeze-dried NPs were treated with 0.5 % (v/v) NaOH in methanol in 37 °C for 48 h to measure the EE by HPLC.

$$\mathrm{EE}(\%) = \frac{\text{amount of drug encapsulated}}{\text{total drug added}} \times 100 \quad (1)$$

2.4.3.3. Drug release. A volume of 1 mL of NPs solution (250 μg/mL) was dialyzed using small volumes tubing (Float-A-Lyzer G2, MWCO: 0.5–1 kDa, SpectrumLabs) against buffer solutions at controlled pH (i.e., 6.4, 7.4 and 8.4). Specifically, buffer solutions at pH 6.4 and pH 7.4 were

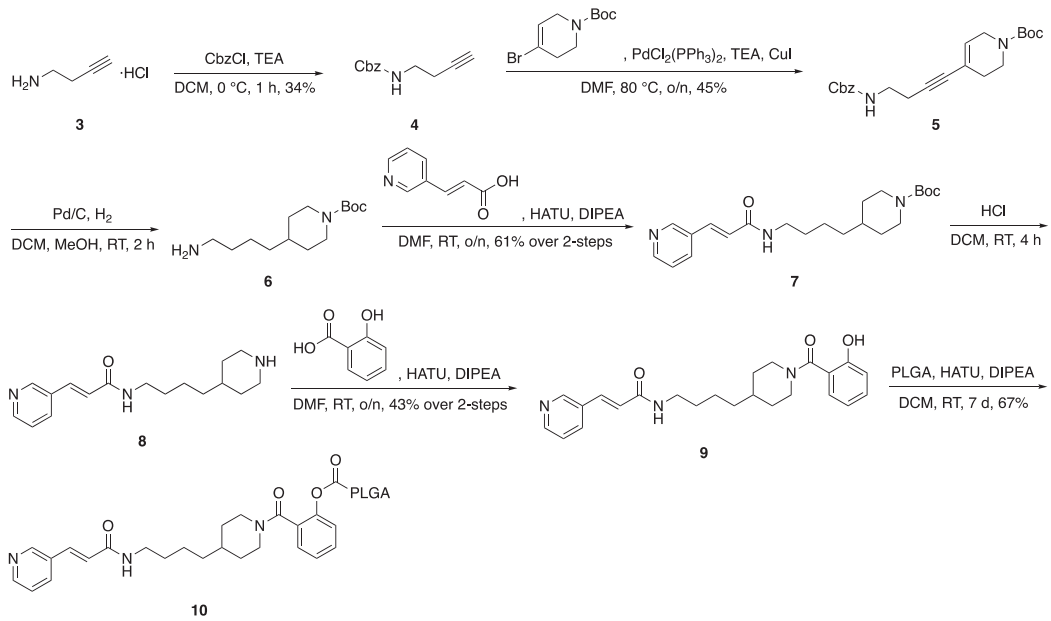

Scheme 2. Synthesis of PLGA polymer conjugated hydroxyl-FK866 (**10**).

prepared with citric acid and Na_2HPO_4; whereas buffer solution at pH 8.4 was prepared with HCl and tris base. In the drug release experiments, each dialysis tubing containing NPs solution was immersed in 5.5 mL of selected buffer and incubated at 37 °C; with buffers changed every 7 days.

2.5. Cell culture

2.5.1. General cell culture

THP-1 and MDA-MB-231 cell lines were kindly donated from Manchester Cancer Research labs (University of Manchester, UK). Unless otherwise specified, all cell culture experiments were performed in a humidified 5 % (v/v) CO_2 air atmosphere at 37 °C in complete medium. Complete medium was prepared supplementing with 10 % (v/v) fetal bovine serum and 2 mM L-glutamine. THP-1 cells were cultured and maintained at densities lower than 1×10^6 cells/mL and discarded upon reaching passage number 20. MDA-MB 231 cells were maintained at densities lower than 5×10^4 cells/cm^2 and discarded upon reaching passage number 25.

2.5.2. Cell proliferation assay

Cell proliferation was determined by measuring cellular mitochondrial metabolic activity using the WST-1 (water soluble tetrazolium) assay at 24 h, 48 h and 72 h. THP-1 and MDA-MB-231 cells were seeded in 96-well plates (3799, Corning Inc., NY, USA) at a density of 10^4 cells/well and 10^4 cells/cm^2, respectively. MDA-MB-231 cells were left adhering overnight. After incubation with NPs or hydroxyl-FK866 at different time points, cells were incubated with WST-1 reagent for 1 h at 37 °C. Untreated cells were used as positive control and used to normalize measured values; whereas cells treated with 30 % (v/v) methanol were used as negative control. Each experiment was performed with $n = 3$ replicates and repeated in $N = 3$ independent experiments. EC_{50} values were calculated with GraphPad Prism (Version 9) using the [non-linear regression, log(inhibitor) response-variable slope] model.

Stocks of hydroxyl-FK866 were dissolved in methanol at a concentration of 1 mg/mL. Stock solutions were filtered using 0.22 μm PVDF filters (Millex-CV, Merck Millipore Ltd. Germany), and then stored at −20 °C until further use. The hydroxyl-FK866 sterile stock solution was diluted in complete media prior each experiment. The same range of drug concentration was used when testing hydroxyl-FK866 loaded NPs.

The concentration of hydroxyl-FK866 loaded in PLGA NPs (i.e. $[\text{hydroxyl-FK866}]_{NP}$) was calculated using the Eq. (2), in which DL(%), and EE(%) were the values previously calculated, $\text{weight}_{\text{hydroxyl-FK866-PLGA}}$ represents the wight of the conjugate, TFR is the total flow rate and $FR_{\text{org.phase}}$ is the flow rate of the organic phase.

$$[hydroxyl-FK866]_{NPs} = \frac{\text{Weight}_{\text{hydroxyl}-FK866-PLGA} \times DL(\%) \times EE(\%) \times FR_{org.phase}}{TFR} \quad (2)$$

2.5.3. Flow cytometry

THP-1 cells and MDA-MB-231 cells in complete medium were seeded in 12 well plates (7.6×10^4 cells/well) and MDA-MB-231 cells were allowed to attach and proliferate overnight under standard sterile conditions for cell culture (5 % CO_2, 37 °C). Cells were then incubated with 125 μg/mL of rhodamine-labeled PLGA [21] NPs in complete medium at 37 °C for 6 h, 24 h and 48 h. Then, MDA-MB-231 cells were washed three times with PBS, detached using trypsin solution (T3942, Sigma-Aldrich, UK) for 3 min at 5 % CO_2, 37 °C. The uptake of the NPs was determined on 2000 individual cells with an Amnis ImageStreamX Mark II Imaging Flow Cytometer (Merck Millipore) equipped with the Amnis INSPIRE software (v200.1.388.0). The emitted signals were collected into channel 405, 488 and 561 nm. The results were analyzed using the Amnis IDEAS software (v6.2.64.0) after gating single cells using the features area and aspect ratio of the bright-field image.

2.6. Molecular docking

The docking simulation of compound **8** were done by following our previous method based on the crystal structures of NAMPT with FK866 (PDB entry: 2GVJ) [22]. FK866 was removed from the crystal structure and all hydrogen atoms added. The chemical structures of compounds **8** was sketched in SYBYL (Tripos, St Louis, MO, USA) and protonated, if appropriate, before energy minimization using the Tripos force field (Gasteiger–Hückel charges, distance-dependent dielectric constant = 4.0, nonbonded interaction cutoff = 8 Å and termination criterion = energy gradient < 0.05 kcal / (mol × Å) for 10,000 iterations). The molecular docking was performed using GOLD Suite 5.1 (Cambridge Crystallographic Data Centre, Cambridge, UK). The original ligand FK866 was extracted, and the new ligands (compound **8**) were fit into the binding pocket of FK866 in NAMPT. The ChemScore and GoldScore

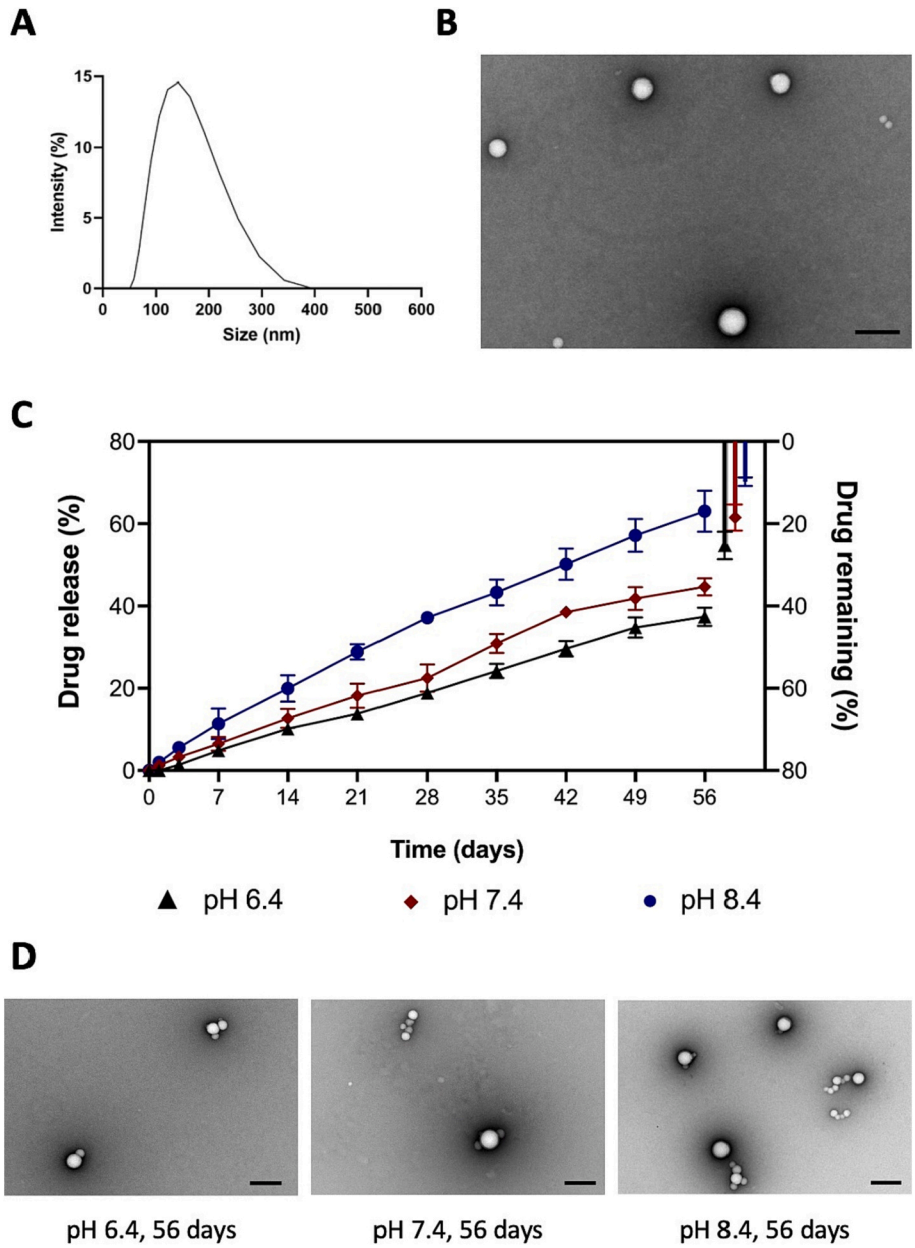

Fig. 8. Hydroxyl-FK866-loaded PLGA nanoparticles prepared by microfluidics system, using 2.5 mg/mL hydroxyl-FK866-PLGA in acetonitrile and 1 % w/v PVA in water with FRR = 1/9, TFR = 200 μL/min, temperature 25 °C. Example of hydroxyl-FK866-PLGA NPs: A) size distribution curve (DLS, 128 ± 8 nm); and B) morphology and size (TEM). C) Release of hydroxyl-FK866 and nanoparticle stability (37 °C, 8 weeks, pH values: 6.4, black triangle; 7.4, red squares; and 8.4, blue circles), and drug remaining amount; D) morphology (shape and size, TEM) of hydroxyl-FK866-loaded PLGA NPs after 56 days incubation in buffer solutions (pH 6.4, pH 7.4 and pH 8.4) Scale bars: 200 nm.

Table 1
Z-average size, PDI and ζ-potential of hydroxyl-FK866-loaded PLGA NPs after 8 weeks incubation at 37 °C and in different pH solution (N = 3 independent experiments).

	pH 6.4	pH 7.4	pH 8.4
Z-average size (nm)	132 ± 5	130 ± 7	134 ± 4
PDI	0.168 ± 0.044	0.173 ± 0.032	0.163 ± 0.028
ζ-potential (mV)	−4.58 ± 0.36	−11.75 ± 0.15	−12.00 ± 1.41

fitness scoring functions were utilized to identify lowest energy binding poses. The exported complexes were edited using UCSF Chimera 1.13.1 software.

2.7. Statistical analysis

All data points on graphs represent the mean of three independent experiments ± standard deviation (st.dev.), unless otherwise stated. Statistical analyses were performed by two-way ANOVA, followed by Sidak's multiple comparison tests in GraphPad Prism 9. Differences were considered significant at $p < 0.05$ (*$p \leq 0.05$, **$p \leq 0.01$, ***$p \leq 0.001$, ****$p \leq 0.0001$).

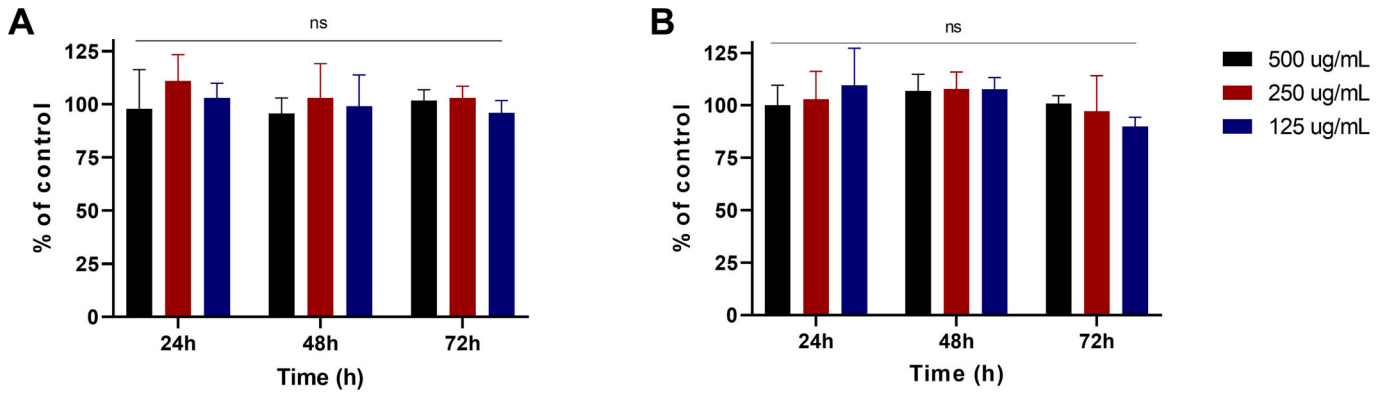

Fig. 9. Cytotoxicity tests (WST-1 assay) using drug-free PLGA NPs: A) THP-1 and B) MDA-MB-231. Cells were incubated with different concentrations of drug-free NPs (125 μg/mL, blue; 250 μg/mL, red; and 500 μg/mL black), with readings at 24 h, 48 h and 72 h. Results are expressed as % compared to untreated cells (control). All data presented as average ± st.dev. ($N = 3$ independent biological triplicates). Differences were considered significant at $p < 0.05$ (*$p \leq 0.05$, **$p \leq 0.01$, ***$p \leq 0.001$, ****$p \leq 0.0001$).

3. Results and discussion

3.1. Synthesis of drug-free PLGA NPs by microfluidics

3.1.1. Effects of microfluidic processing parameters on size and polydispersity index (PDI) of drug-free PLGA nanoparticles

Negatively charged PLGA NPs with size between 50 nm and 250 nm were produced (Fig. 3) by varying the selected manufacturing parameters (FRR, TFR, PLGA and PVA concentration). We found that manufacturing parameters impact of the characteristics of obtained particles, with the FRR positively correlated with particles size (Fig. 3A, C). Of note, the PDI was found to be always in the range of 0.1–0.3, showing robustness and reproducibility of the microfluidic system for this manufacturing process. Notably, the presence of PVA affects the size of PLGA nanoparticles. Without PVA, smaller variations in nanoparticle size and PDI are observed when the FRR and PLGA concentrations were increased from 1/19 to 1/1.5 and 2.5 mg/mL to 5 mg/mL, respectively (Fig. 3A, C). The presence of PVA (1 % w/v) instead returns statistically different variations of PLGA NPs' size as function of the manufacturing parameters used. Quantitatively, linear programming of size and FRR was conducted, in the group with PVA (Fig. 3C), the slopes of the 2.5 mg/mL and 5 mg/mL groups were 165.62 and 162.92, respectively; while in the group without PVA, the number are 8.99 and 64.81, respectively. When applying PVA, the positive correlation between Z-average size of PLGA NPs and the FRR was also confirmed using a PLGA with higher Mw (RG502H, Mw 7000–17,000, 2.5 mg/mL in acetonitrile, Supplementary material Fig. S1). Additionally, higher concentration of PLGA in acetonitrile (5 mg/mL) returns larger NPs, being on average 28 ± 5 nm larger than those manufactured with lower PLGA concentration while using the same TFR and FRR (2.5 mg/mL, Fig. 3C). This is thought to occur because the higher quantity of PLGA monomers lead to slower solvent diffusion and therefore larger particle size [11], as reported previously by Karnik et al. [11], Hung et al. [12], Rezvantalab and Keshavarz Moraveji [9]. Of note, with FRR = 1/9, variations of the TFR did not impact on the Z-average size and PDI of produced PLGA NPs; with or without PVA as surfactant (Fig. 3B, D). This could explained by the fact that acetonitrile/water balance at the mixing point did not change as function of the TFR, as reported in literature [23,24]. Importantly, these results confirmed that the molecular weight and composition of PLGA does not impact on NPs size, which instead can be controlled by varying manufacturing parameters such as FRR, presence of PVA and concentration of PLGA.

3.1.2. Effects of microfluidic processing parameters on ζ-potential of drug-free PLGA NPs

ζ-Potential is the scientific term for electromotive force in colloidal systems and an important particle characteristic to describe the charge at the nanoparticle's surface. The ζ-potential value is reported to influence NPs stability and activity in biological aqueous environments (e.g. nanoparticle mucosal adhesion, formation of protein corona in blood circulation) [25]. ζ-Potential values of the PLGA NPs prepared in this study vary between −12 and −51 mV, depending on the presence or not of PVA. All the NPs herein manufactured have negative ζ-potential values, this is due to the presence of uncapped end carboxyl groups in the PLGA polymer used in this study. Varying TFR and FRR did not significantly impact on the measured ζ-potential values in the absence of PVA. Instead, variations of ζ-potential were observed in PLGA NPs coated with PVA. At higher FRR, more PLGA and less water/PVA in water are mixed in the chip junction, leading to a higher negative charge of produced nanoparticles (Fig. 4A, C). This result is also confirmed while using PLGA with different Mw (Supplementary material Fig. S2). Fig. 4A shows that the plain NPs (PLGA without PVA) have the ζ-potential between −40 mV and −50 mV, similar to what previously reported [23]. The presence of a coating (such as PVA) on PLGA NPs is known to change the ζ-potential values between coated and uncoated NPs [24,26]. In this study, the presence of PVA coating on PLGA NPs cause the increase of the surface charge, with measured ζ-potential between −10 mV and −25 mV (Fig. 4D). Of note, and similarly to what observed previously on size and PDI, variations of the TFR do not significantly change ζ-potential values (Fig. 4B, D). After these results, [PLGA] = 2.5 mg/mL, FRR = 1/9, TFR = 200 μL/min and a temperature of 25 °C were the selected manufacturing parameters to meet the PLGA NPs requirements (100–150 nm, PDI < 0.2, negative charge). All the NPs referred to from now on were fabricated using these parameters.

3.1.3. Size stability of drug-free PLGA NPs kept at 4 °C

The size and shape stability of PLGA NPs was monitored at 4 °C and pH 7.4 up to 4 weeks, measuring Z-average size, PDI and ζ-potential. The results show no significant variation of observed properties up to 4 weeks in all NPs (Fig. 5).These size stability tests are particularly important for evaluating the properties of NPs, as well as possible aggregations, ensuring predicted dissolution kinetics [27].

TEM images (Fig. 6) show that PLGA NPs fabricated using microfluidics are spherical and have a smooth surface, regardless the presence or not of PVA. Whereas the size obtained by TEM has two populations for each sample, one is similar to that obtained by DLS, but slightly smaller than the size measured by DLS (Supplementary materials Fig. S3). This is because TEM provides information about the size and shape of individual nanoparticles dried on a substrate under high vacuum, and DLS measures the size of hydrated particles in water suspension. Differences in nanoparticles size measure by TEM and DLS are often reported in literature [28]. A smaller nanoparticles population

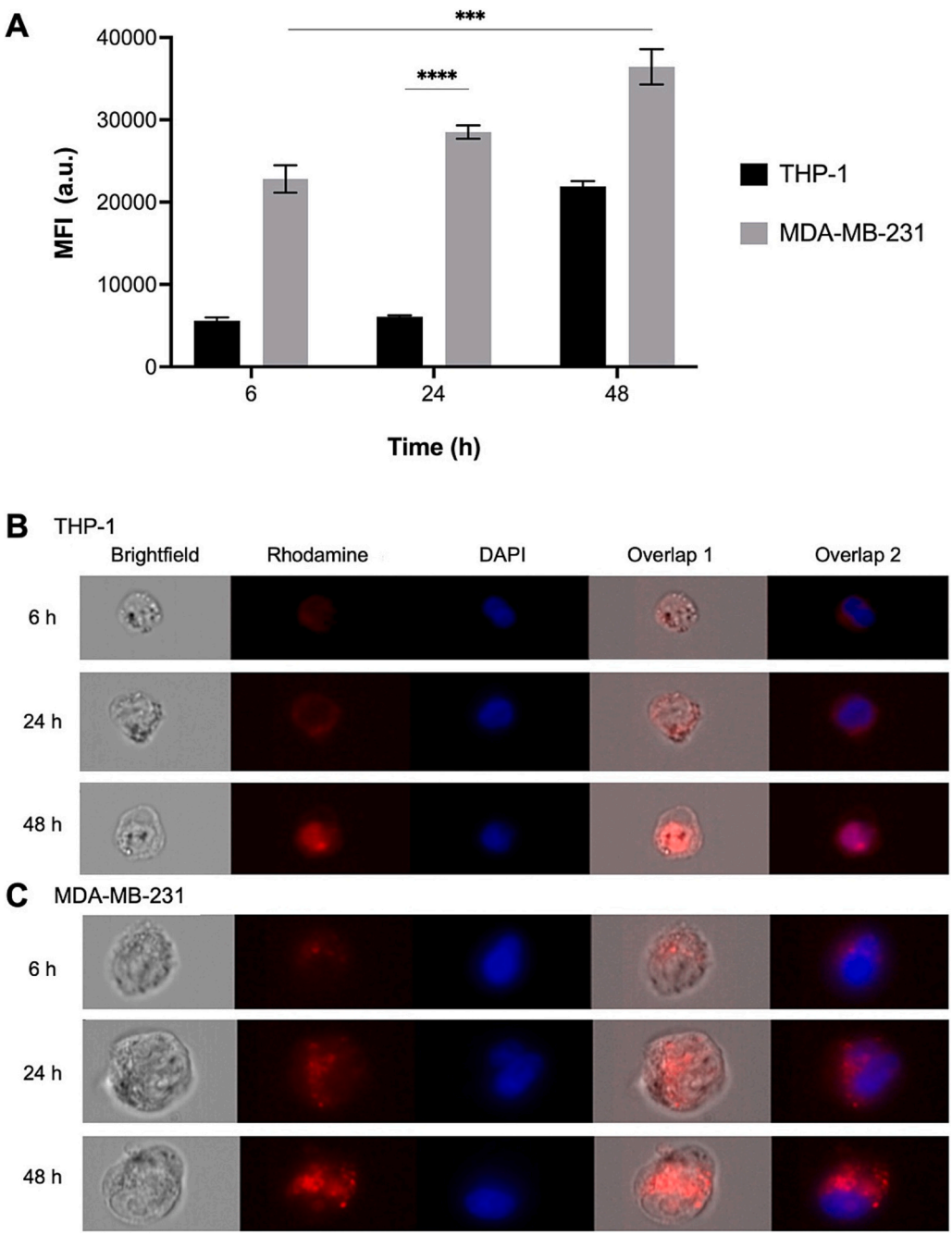

Fig. 10. Internalization of rhodamine-PLGA NPs (125 μg/mL; 6, 24 and 48 h): A) median fluorescence intensity (MFI) obtained through flow cytometry analysis of THP-1 and MDA-MB-231. Representative images displayed as bright field, cell nucleus (DAPI, blue), NPs (rhodamine-PLGA NPs, red) and overlaps of: B) THP-1 cells; and C) MDA-MB-231. Of note, the rhodamine used in this study is conjugated to PLGA polymer, therefore, the detection of fluorescence in the cells can be considered to be that of the rhodamine associated with the PLGA NPs and not any leached rhodamine. Data presented as average ± st.dev. ($N = 2$ independent biological duplicates). Differences were considered significant at $p < 0.05$ (*$p \leq 0.05$, **$p \leq 0.01$, ***$p \leq 0.001$, ****$p \leq 0.0001$).

with average size of approx. 20 nm (black arrow in Fig. 6), are not present in DLS measurement (all samples have single-peak distribution in Z-average size plots). This phenomenon could be attributed to the measurement principle of DLS, which converts the fluctuation of scattered light into a correlation function and in the Rayleigh approximation, the intensity of the scattered light of the particles is directly proportional to the diameter by the power of 6, so that the contribution of the total scattered light by small particles is insignificant in the presence of big particles [29].

Based on the results, microfluidic is proven a suitable manufacturing method to control the size of NPs. This adds to the other advantages of high production efficiency and in short period of time, essential feature in manufacturing high-quality NPs for controlled drug release. In fact, microfluidics allows manufacturing within seconds (at the junction) with overall production time adjusted based on the selected flow rates [30]. When compared to batch methods (e.g. 18 h for the production of silica NPs in batch reactors), the production time of microfluidics could be 10 times shorter than conventional method [31]. The production efficiency in our study is 32.16 mg of PLGA NPs per hour, which could be further improved (higher mass production over time) by optimizing the parameters, such as the initial concentration and FRR.

Table 2
EC_{50} and E_{max} values for THP-1 cells and MDA-MB-231 cells treated with hydroxyl-FK866 and hydroxyl-FK866-PLGA NPs (24 h, 48 h and 72 h) measured by WST-1 assay. Data presented as average ± st.dev. ($N = 3$ independent biological triplicates).

		THP-1		MDA-MB-231	
		EC_{50} (nM)	E_{max}	EC_{50} (nM)	E_{max}
Hydroxyl-FK866	24 h	1.04 ± 0.09	41.93 ± 4.22 %	3.14 ± 1.90	50.86 ± 2.00 %
	48 h	1.98 ± 0.79	21.63 ± 2.90 %	10.90 ± 4.31	20.86 ± 0.66 %
	72 h	2.09 ± 0.10	19.43 ± 0.74 %	N/A	
Hydroxyl-FK866-PLGA nanoparticles	24 h	4.74 ± 0.97	49.20 ± 3.84 %	49.07 ± 14.29	69.76 ± 8.22 %
	48 h	2.47 ± 0.02	19.35 ± 0.81 %	72.35 ± 4.56	48.88 ± 2.46 %
	72 h	2.76 ± 0.23	16.89 ± 0.52 %	N/A	

N/A: data not available.

3.2. Design and synthesis of hydroxyl-FK866 conjugates

In order to design a conjugate between a NAMPT inhibitor (FK866) and PLGA we considered both the likely stability of the conjugation site and the ability of the cleavage product to effectively inhibit NAMPT. We considered that a phenolic ester linkage was likely to provide a suitable hydrolysis, with the solvent exposed benzoyl amide likely to provide a suitable site for introduction of the hydroxyl group required for this conjugation. To verify our designing rational, we first made two model compounds (**1** and **2**, Scheme 1) to assess the ester bond hydrolysis under different conditions, confirming that the ester bond in both model compounds were able to be hydrolyzed (Supplementary materials, Fig. S4) with similar profiles observed between **1** and **2**.

To avoid any influence regarding potency of the hydroxyl group introduced to allow conjugation, we conducted some docking simulations based on the published co-crystal structure between FK866 and NAMPT (PDB entry: 2GVJ). As shown in Fig. 7A, this docking study showed that both FK866 (in cream spheres) and the ortho-hydroxyl modified FK866 were located in identical binding site with and identical hydrogen bonding pattern towards Ser275 and water molecular 1339 (Fig. 7C). Meanwhile, as expected OH group is pointing towards solvent and is therefore unlikely to interfere significantly with the potency of the ligand (Fig. 7B).

To synthesize hydroxy-FK866 and the PLGA conjugate, we utilized Cbz group protection of commercially available but-3-yn-1-amine hydrochloride prepare alkyne **4**, which allowed us to access intermediate **5** through a Sonogashira reaction, with subsequent hydrogenation affording **6** (Scheme 2). Amine **6** was converted to the advanced intermediate 8 by coupling and subsequent deprotection under acidic conditions, which was converted to the desired hydroxyl-FK866 **8** by amide coupling (Scheme 2). Similar to the synthesis of previous model compound, we were able to achieve the FK866 conjugated PLGA polymer **8** via a coupling reaction (Scheme 2).

3.3. Fabrication and physicochemical properties of hydroxyl-FK866 loaded PLGA NPs

3.3.1. Size, uniformity, surface charge and morphology

PLGA drug-loaded NPs were prepared targeting a size in the range of 100–200 nm, allowing circulation and clearance [32–34]. As previously discussed, FRR = 1/9, TFR = 200 μL/min and temperature of 25 °C were the selected manufacturing parameters, using hydroxyl-FK866-PLGA at concentration of 2.5 mg/mL in acetonitrile (organic phase) and 1 % w/v PVA solution (aq.) (aqueous phase). As shown in Fig. 8, hydroxyl-FK866-loaded NPs are mono-distributed with Z-average size of 128 ± 8 nm (PDI 0.135 ± 0.087) and ζ-potential −14.8 ± 5.3 mV (Supplementary materials Fig. S5), results confirmed by TEM showing round-shaped and homogeneous NPs. Results confirmed that selected manufacturing parameters allows fabrication of NPs with target size, confirming what previously observed for drug-free PLGA NPs, confirming the suitability of microfluidics for a high-throughput fabrication of PLGA-based NPs.

3.3.2. Encapsulation efficiency (EE) and in-vitro drug release profile

Based on the experimental design of the conjugate hydroxyl-FK866-PLGA NPs, the theoretical EE to be achieved is 100 %. Measured encapsulation efficiency of hydroxyl-FK866 returned a value of 98.6 ± 5.8 %; confirming the proposed manufacturing process as a feasible approach to overcome common issues reported in literature of poor drug encapsulation in PLGA NPs (typically lower than 70 % [35]). Drug loading (DL%) is typically lower than EE, due to the difference in molecular weight of PLGA and the selected drug; generally reported as 1 % in the relatively high EE NPs [35]. In this study, the DL% of all batches is higher than 2 %. As a result, this fabrication method enhances both EE and DL%.

The second common problem reported in polymeric NPs is the initial burst release [35–37]. For example, docetaxel-loaded PLGA NPs (EE 23.09 ± 1.3 %), showed 68 % release within the first 24 h [38]. This initial burst of the drug is normally undesirable because it shortens the overall duration of the therapeutic effect, and excessive burst may even cause toxicity raising safety concerns [35,39]. To reduce the initial burst release and maximize the duration of drug action [39,40], the hydroxyl-FK866-PLGA was designed to hydrolyze with slow kinetic and as function of the pH value, enabling hydroxyl-FK866-PLGA NPs to release the active compound over a prolonged period of time (up to 3 months). As shown in Fig. 8C, a long-sustained release pattern and without any initial burst release was observed in all conditions tested (pH 6.4–8.4). Moreover, and as by design, hydroxyl-FK866 was released faster when NPs were incubated in a basic buffer (pH 8.4) compared to the acidic conditions (pH 6.4). These results confirmed our initial hypothesis to obtain a drug release rate depending not only on the diffusion of the drug from the nanoparticle matrix, but mainly on the hydrolysis between hydroxyl-FK866 and PLGA. After two months (37 °C, buffered condition), and at the selected end point, NPs were recovered and disrupted to quantify the remaining hydroxyl-FK866. It was found that a smaller amount of hydroxyl-FK866 in particles incubated at pH 8.4 (9.63 ± 1.34 %) than in the ones incubated at pH 6.4 (25.26 ± 2.70 %) (Fig. 8C). At the same time, the Z-average size and PDI of NPs were measured over time and no significant variations were found in all conditions tested (Supplementary material Figs. S5 and S6), with a reported average size of 131 ± 6 nm (PDI 0.167 ± 0.044). Interestingly, the ζ-potential of NPs incubated at pH 7.4 and pH 8.4 was found more negative than values measured in acidic condition (Table 1), consistent with what reported in literature [41,42]. Even for ζ-potential, no variations were recorded over the monitored time. Finally, the morphology of nanoparticles was maintained spherical and with smooth surfaces in all conditions tested and up to the end point (Fig. 8D, Supplementary material Fig. S7).

3.4. In-vitro efficacy of hydroxyl-FK866 free/loaded nanoparticles in tumor cell lines

3.4.1. Toxicity of drug-free NPs

Both PLGA and PVA, used for manufacturing of nanoparticles in this study, are biodegradable, biocompatible, non-toxic and FDA approved [35,43]. Cytotoxicity of drug-free PLGA nanoparticle was evaluated using a human leukemia cell line (THP-1) and a breast cancer cell line (MDA-MB-231). Cell proliferation was measured using the WST-1 assay for both cell lines, testing different NPs concentrations (125, 250 and 500 μg/mL) up to 72 h of incubation (Fig. 9). In addition, cell count and morphology were observed over time for THP-1 cells to evaluate

proliferation, as well as possible monocytes differentiation (Supplementary materials, Fig. S8). Incubation with drug-free PLGA NPs did not show any toxicity on both THP-1 and MDA-MB-231 cells, even at the highest concentration of drug-free PLGA NPs used (i.e. 500 μg/mL), and when compared to un-treated control group at each time point for 24 h, 48 h and 72 h in both cell lines tested (Fig. 9). In some cases, NPs-treated cells showed increased proliferation when compared to untreated cells (control). Similar results were reported in literatures [44,45], suggesting that the interaction with lactic acid and/or inert NPs may increase the proliferation rate [46]. Of note, this slight increase in cells viability (WST-1 assay) is not significant across all the conditions tested, confirming the cytocompatibility up to 72 h of drug-free PLGA NPs for both THP-1 and MDA-MB-231 cells.

3.4.2. Toxicity of hydroxyl-FK866 and hydroxyl-FK866-PLGA NPs

After assessing the cytocompatibility of drug-free PLGA NPs (Fig. 10), cells were treated with free hydroxyl-FK866 and hydroxyl-FK866-loaded NPs to quantify toxicity in both THP-1 and MDA-MB-231 cells. WST-1 assay was selected as more sensitive to NADH/NAD+ variations as FK866 can interfere with the biosynthesis of the coenzyme NAD+ [15,47]. EC_{50} (concentration giving 50 % of maximum response) and E_{max} (maximum percent signal reduction as defined by lower asymptote) values were calculated using WST-1 plots (Supplementary material Figs. S9, S10), and summarized in Table 2. Of note, EC_{50} values of free hydroxyl-FK866 on THP-1 cells aligns with the results obtained in other studies [48] and in the range of 1–2 nM; whereas slightly higher values were obtained using hydroxyl-FK866-loaded NPs (i.e. 2–5 nM). This could be due to the fact that hydroxyl-FK866 is slowly released in the cell culture media, as shown in Fig. 8. It is possible to overcome this and have a comparable toxicity to the free drug, by loading more drug in nanoparticles. In the case of MDA-MB-231 cells, toxicity of free hydroxyl-FK866 and hydroxyl-FK866 loaded NPs did not align as observed in THP-1 cells. As expected, and reported in literature, free hydroxyl-FK866 is less toxic in MDA-MB-231 when compared to THP-1. In the case of incubation with hydroxyl-FK866-PLGA NPs, due to the slow release of hydroxyl-FK866 (Fig. 9) even lower toxicity was recorded. In addition, it showed that longer treatment time results in the higher E_{max} with less cell proliferation, for example, when treating THP-1 cells by hydroxyl-FK866-PLGA NPs, the E_{max} for 72 h is 16.89 ± 0.52 %, compared to 41.93 ± 4.22 % during 24 h, the more efficiency of longer time treatment means less cell proliferation.

3.5. Nanoparticle internalization: rhodamine-labeled PLGA nanoparticles

To better understand cytotoxicity results, rhodamine-labeled PLGA NPs were used to study the kinetics of NPs internalization in both THP-1 and MDA-MB-231 cells. Rhodamine-labeled PLGA NPs were prepared using the selected manufacturing parameters, and obtaining nanoparticles with Z-average size of 124 ± 7 nm (PDI 0.176 ± 0.038) and ζ-potential of −15.1 ± 3.8 mV (Supplementary material Fig. S11). NPs were found similar to PLGA and hydroxyl-FK866-PLGA NPs, confirming the high reproducibility of the fabrication method (Figs. 3 and 4), as well as their suitability (size, surface charge and morphology) for internalization tests. Internalization of NPs was evaluated at a concentration of 125 μg/mL (as per toxicity tests) and at different incubation times (6 h, 24 h and 48 h) by flow cytometry, in both THP-1 and MDA-MB-231 cells (Fig. 10).

After 48 h incubation, more NPs were internalized in both cell lines tested. Results evidenced a slower nanoparticle internalization rate in THP-1 cells when compared to MDA-MB 231, at any time point (Fig. 10A). Of note, very few NPs were internalized in THP-1 within the first 24 h of incubation, with no statistical difference between 6 h and 24 h. This suggests that hydroxyl-FK866 is predominantly released extracellularly in the first 24 h, showing higher potency in THP-1 than in MDA-MB-231. After 48 h incubation, approx. 4-fold increase of internalized NPs was measured and when compared to earlier time points (Fig. 10A).

NPs uptake in MDA-MB-231 cells was found much higher than THP-1; difference notable from the early time points (6 h). Internalization of NPs in MDA-MB-231 increased linearly over time and up to 48 h (end point). Interestingly, we observed that the higher internalization of NPs (in MDA-MB-231 cells) corresponds to the lower cytotoxicity detected (Table 2). It is possible to hypothesize that greater internalization in MDA-MB-231, could hinder the release of hydroxyl-FK866 intracellularly (for example a slower release may occur in lysosomes, where the pH is <5), hence have a reduced cytotoxicity overall. On the contrary, when NPs are not internalized (THP-1), hydroxyl-FK866 is released in the cell culture media (pH = 7.2) with direct effect to cells. In specific, higher EC_{50} values are reported at later time points (48 and 72 h) and as hydroxyl-FK866 is slowly released in the cell culture media (Figs. 8C and 9A). In the context of the slow extracellular release of hydroxyl-FK866, it is possible to predict an increased toxicity over time, in-line with release of tolerated doses and with the potential on clinical use of the studied NPs. Moreover, from the presented results, it is possible to conclude that the higher internalization does not strictly mean higher toxicity with this type of nanoparticles. Again, this supports the design criteria of NPs as reservoir of potent toxins, able to slowly release low doses at the site of intervention.

4. Conclusions

In this study, we synthesized PLGA-based NPs with known size, surface charge, shape, and drug loading using a microfluidic system. The PLGA concentration, FRR, TFR, and the presence of PVA as surfactant affect the size and surface charge of NPs. Optimized fabrication parameters of microfluidic systems enable precise and rapid fabrication of different nanoparticles with known physicochemical properties. A hydroxyl-FK866 conjugated PLGA polymer was prepared by a coupling reaction for the preparation of drug-loaded nanoparticles with selected fabrication parameters, obtaining nanoparticles with Z-average size = 128 ± 8 nm, PDI = 0.135 ± 0.087, and ζ- Potential = −14.8 ± 5.3 mV with known drug (hydroxyl-FK866) content. Cytotoxicity tests and cell internalization of hydroxyl-FK866-PLGA nanoparticles were performed in THP-1 and MDA-MB-231 cells, where the higher toxic effect was observed in THP-1 cells. It is worth noting that, according to our knowledge, this is the first NAMPT inhibitor conjugated PLGA nanoparticles reported in the literature as therapeutic agent. Hydroxyl-FK866-PLGA nanoparticles have high EE = 98.6 ± 5.8 %, solving typical problems reported in drug loaded polymeric NPs [35]. Moreover, hydroxyl-FK866-PLGA NPs showed a sustained drug release over 2 months in physiological conditions, avoiding the common burst release and undesired biphasic release pattern problems reported in literature. Paving new formulation and fabrication strategies to solve safety concerns linked to drug toxicity [3]. Hydroxyl-FK866-PLGA NPs have the potential to 1) reduce concentration fluctuation in steady-state drug levels, minimize "peak and valley" pattern, increase the safety; 2) decrease drug administration and treatment period, improve patients' compliance; 3) maximum utilization of drug, increase safety margin of drug and decrease therapeutic costs; and 4) better life-cycle management of drugs, extended relief of symptoms [3]. In conclusion, the herein proposed PLGA-based NPs open a new paradigm on the fabrication of polymeric NPs using microfluidic, knowing precisely the amount of drug loaded in the polymeric NPs and achieve a pH-dependent prolonged sustained release to increase efficacy of therapeutic agents.

CRediT authorship contribution statement

Xue Bai: Conceptualization, Methodology, Validation, Formal analysis, Investigation, Writing – original draft, Writing – review & editing, Visualization. **Siyuan Tang:** Methodology, Validation, Formal analysis, Writing – review & editing. **Sam Butterworth:** Conceptualization, Data curation, Writing – review & editing, Supervision, Funding

acquisition. **Annalisa Tirella:** Conceptualization, Formal analysis, Data curation, Writing – review & editing, Visualization, Supervision, Funding acquisition.

Declaration of competing interest

The authors declare that they have no known competing financial interests or personal relationships that could have appeared to influence the work reported in this paper.

Data availability

Data will be made available on request.

Acknowledgements

The authors would like to thank flow cytometry core facility and electron microscopy core facility in FBMH at the University of Manchester. Dr. Xue Bai would like to thank Dr. Leonidas Gkionis, Dr. Lekha Shah and Dr. Ponpawee Pingrajai for the help with microfluidics and cell culture experiments.

Funding

Dr. Siyuan Tang was funded by the China Sponsorship Council (No. 201709110169).

Appendix A. Supplementary data

Supplementary data to this article can be found online at https://doi.org/10.1016/j.bioadv.2023.213649.

References

[1] Cancer, (n.d.). https://www.who.int/news-room/fact-sheets/detail/cancer (accessed January 4, 2022).
[2] R. Buono, V. Longo, Starvation, stress resistance, and cancer, Trends Endocrinol. Metab. 29 (2018), https://doi.org/10.1016/j.tem.2018.01.008.
[3] X. Bai, Z.L. Smith, Y. Wang, S. Butterworth, A. Tirella, Sustained drug release from smart nanoparticles in cancer therapy: a comprehensive review, Micromachines (Basel) 13 (2022) 1623, https://doi.org/10.3390/mi13101623.
[4] H.K. Makadia, S.J. Siegel, Poly lactic-co-glycolic acid (PLGA) as biodegradable controlled drug delivery carrier, Polymers 3 (2011) 1377–1397, https://doi.org/10.3390/polym3031377.
[5] L. Gkionis, H. Aojula, L.K. Harris, A. Tirella, Microfluidic-assisted fabrication of phosphatidylcholine-based liposomes for controlled drug delivery of chemotherapeutics, Int. J. Pharm. 604 (2021) 120711, https://doi.org/10.1016/j.ijpharm.2021.120711.
[6] G.M. Whitesides, The origins and the future of microfluidics, Nature 442 (2006) 368–373, https://doi.org/10.1038/nature05058.
[7] J.P. Martins, G. Torrieri, H.A. Santos, The importance of microfluidics for the preparation of nanoparticles as advanced drug delivery systems, Expert Opin. Drug Deliv. 15 (2018) 469–479, https://doi.org/10.1080/17425247.2018.1446936.
[8] S. Garg, G. Heuck, S. Ip, E. Ramsay, Microfluidics: a transformational tool for nanomedicine development and production, J. Drug Target. 24 (2016) 821–835, https://doi.org/10.1080/1061186X.2016.1198354.
[9] S. Rezvantalab, M.K. Moraveji, Microfluidic assisted synthesis of PLGA drug delivery systems, RSC Adv. 9 (2019) 2055–2072, https://doi.org/10.1039/C8RA08972H.
[10] P. Zhu, L. Wang, Passive and active droplet generation with microfluidics: a review, Lab Chip 17 (2017) 34–75, https://doi.org/10.1039/C6LC01018K.
[11] R. Karnik, F. Gu, P. Basto, C. Cannizzaro, L. Dean, W. Kyei-Manu, R. Langer, O. C. Farokhzad, Microfluidic platform for controlled synthesis of polymeric nanoparticles, Nano Lett. 8 (2008) 2906–2912, https://doi.org/10.1021/nl801736q.
[12] L.-H. Hung, S.-Y. Teh, J. Jester, A.P. Lee, PLGA micro/nanosphere synthesis by droplet microfluidic solvent evaporation and extraction approaches, Lab Chip 10 (2010) 1820–1825, https://doi.org/10.1039/C002866E.
[13] N. Lababidi, V. Sigal, A. Koenneke, K. Schwarzkopf, A. Manz, M. Schneider, Microfluidics as tool to prepare size-tunable PLGA nanoparticles with high curcumin encapsulation for efficient mucus penetration, Beilstein J. Nanotechnol. 10 (2019) 2280–2293, https://doi.org/10.3762/bjnano.10.220.
[14] M. Bellone, A. Calcinotto, P. Filipazzi, A. De Milito, S. Fais, L. Rivoltini, The acidity of the tumor microenvironment is a mechanism of immune escape that can be overcome by proton pump inhibitors, Oncoimmunology 2 (2013), e22058, https://doi.org/10.4161/onci.22058.
[15] K. Holen, L.B. Saltz, E. Hollywood, K. Burk, A.-R. Hanauske, The pharmacokinetics, toxicities, and biologic effects of FK866, a nicotinamide adenine dinucleotide biosynthesis inhibitor, Investig. New Drugs 26 (2008) 45–51, https://doi.org/10.1007/s10637-007-9083-2.
[16] C.S. Neumann, K.C. Olivas, M.E. Anderson, J.H. Cochran, S. Jin, F. Li, L.V. Loftus, D.W. Meyer, J. Neale, J.C. Nix, P.G. Pittman, J.K. Simmons, M.L. Ulrich, A. B. Waight, A. Wong, M.C. Zaval, W. Zeng, R.P. Lyon, P.D. Senter, Targeted delivery of cytotoxic NAMPT inhibitors using antibody-drug conjugates, Mol. Cancer Ther. 17 (2018) 2633–2642, https://doi.org/10.1158/1535-7163.MCT-18-0643.
[17] N. Böhnke, M. Berger, N. Griebenow, A. Rottmann, M. Erkelenz, S. Hammer, S. Berndt, J. Günther, A.M. Wengner, B. Stelte-Ludwig, C. Mahlert, S. Greven, L. Dietz, H. Jörißen, N. Barak, U. Bömer, R.C. Hillig, U. Eberspaecher, J. Weiske, A. Giese, D. Mumberg, C.F. Nising, H. Weinmann, A. Sommer, A novel NAMPT inhibitor-based antibody–drug conjugate payload class for cancer therapy, Bioconjug. Chem. 33 (2022) 1210–1221, https://doi.org/10.1021/acs.bioconjchem.2c00178.
[18] D.R. Lee, J.S. Park, I.H. Bae, Y. Lee, B.M. Kim, Liquid crystal nanoparticle formulation as an oral drug delivery system for liver-specific distribution, Int. J. Nanomedicine 11 (2016) 853–871, https://doi.org/10.2147/IJN.S97000.
[19] Z. Wen, Z. Yan, K. Hu, Z. Pang, X. Cheng, L. Guo, Q. Zhang, X. Jiang, L. Fang, R. Lai, Odorranalectin-conjugated nanoparticles: preparation, brain delivery and pharmacodynamic study on Parkinson's disease following intranasal administration, J. Control. Release 151 (2011) 131–138, https://doi.org/10.1016/j.jconrel.2011.02.022.
[20] N.N. Pardeshi, W. Qi, K. Dahl, L. Caplan, J.F. Carpenter, Microparticles and nanoparticles delivered in intravenous saline and in an intravenous solution of a therapeutic antibody product, J. Pharm. Sci. 106 (2017) 511–520, https://doi.org/10.1016/j.xphs.2016.09.028.
[21] J.M. Rios De La Rosa, A. Spadea, R. Donno, E. Lallana, Y. Lu, S. Puri, P. Caswell, M. J. Lawrence, M. Ashford, N. Tirelli, Microfluidic-assisted preparation of RGD-decorated nanoparticles: exploring integrin-facilitated uptake in cancer cell lines, Sci. Rep. 10 (2020) 14505, https://doi.org/10.1038/s41598-020-71396-x.
[22] S. Tang, M. Garzon Sanz, O. Smith, A. Krämer, D. Egbase, P.W. Caton, S. Knapp, S. Butterworth, Chemistry-led investigations into the mode of action of NAMPT activators, resulting in the discovery of non-pyridyl class NAMPT activators, Acta Pharm. Sin. B (2022), https://doi.org/10.1016/j.apsb.2022.07.016.
[23] S.K. Sahoo, J. Panyam, S. Prabha, V. Labhasetwar, Residual polyvinyl alcohol associated with poly (d,l-lactide-co-glycolide) nanoparticles affects their physical properties and cellular uptake, J. Control. Release 82 (2002) 105–114, https://doi.org/10.1016/S0168-3659(02)00127-X.
[24] M. Yang, S.K. Lai, T. Yu, Y.-Y. Wang, C. Happe, W. Zhong, M. Zhang, A. Anonuevo, C. Fridley, A. Hung, J. Fu, J. Hanes, Nanoparticle penetration of human cervicovaginal mucus: the effect of polyvinyl alcohol, J. Control. Release 192 (2014) 202–208, https://doi.org/10.1016/j.jconrel.2014.07.045.
[25] S. Honary, F. Zahir, Effect of zeta potential on the properties of nano-drug delivery systems - a review (part 1), Trop. J. Pharm. Res. 12 (2013) 255–264, https://doi.org/10.4314/tjpr.v12i2.19.
[26] O. Mert, S.K. Lai, L. Ensign, M. Yang, Y.-Y. Wang, J. Wood, J. Hanes, A poly (ethylene glycol)-based surfactant for formulation of drug-loaded mucus penetrating particles, J. Control. Release 157 (2012) 455–460, https://doi.org/10.1016/j.jconrel.2011.08.032.
[27] J. Feng, Y. Zhang, S.A. McManus, K.D. Ristroph, H.D. Lu, K. Gong, C.E. White, R. K. Prud'homme, Rapid recovery of clofazimine-loaded nanoparticles with long-term storage stability as anti-cryptosporidium therapy, ACS Appl. Nano Mater. 1 (2018) 2184–2194, https://doi.org/10.1021/acsanm.8b00234.
[28] T. Ito, Li Sun, M. Bevan, R. Crooks, Comparison of nanoparticle size and electrophoretic mobility measurements using a carbon-nanotube-based coulter counter, dynamic light scattering, transmission electron microscopy, and phase analysis light scattering, Langmuir 20 (2004) 6940–6945, https://doi.org/10.1021/la049524t.
[29] C. Troiber, J.C. Kasper, S. Milani, M. Scheible, I. Martin, F. Schaubhut, S. Küchler, J. Rädler, F.C. Simmel, W. Friess, E. Wagner, Comparison of four different particle sizing methods for siRNA polyplex characterization, Eur. J. Pharm. Biopharm. 84 (2013) 255–264, https://doi.org/10.1016/j.ejpb.2012.08.014.
[30] S.J. Shepherd, D. Issadore, M.J. Mitchell, Microfluidic formulation of nanoparticles for biomedical applications, Biomaterials 274 (2021) 120826, https://doi.org/10.1016/j.biomaterials.2021.120826.
[31] X. Li, X. Jiang, Microfluidics for producing poly (lactic-co-glycolic acid)-based pharmaceutical nanoparticles, Adv. Drug Deliv. Rev. 128 (2018) 101–114, https://doi.org/10.1016/j.addr.2017.12.015.
[32] J. Rao, Shedding light on tumors using nanoparticles, ACS Nano 2 (2008) 1984–1986, https://doi.org/10.1021/nn800669n.
[33] D.E. Owens, N.A. Peppas, Opsonization, biodistribution, and pharmacokinetics of polymeric nanoparticles, Int. J. Pharm. 307 (2006) 93–102, https://doi.org/10.1016/j.ijpharm.2005.10.010.
[34] W.B. Liechty, N.A. Peppas, Expert opinion: responsive polymer nanoparticles in cancer therapy, Eur. J. Pharm. Biopharm. 80 (2012) 241–246, https://doi.org/10.1016/j.ejpb.2011.08.004.
[35] F. Danhier, E. Ansorena, J.M. Silva, R. Coco, A. Le Breton, V. Préat, PLGA-based nanoparticles: an overview of biomedical applications, J. Control. Release 161 (2012) 505–522, https://doi.org/10.1016/j.jconrel.2012.01.043.
[36] R.H. Ansary, M.B. Awang, M.M. Rahman, Biodegradable poly(D,L-lactic-co-glycolic acid)-based micro/nanoparticles for sustained release of protein drugs - a review, Trop. J. Pharm. Res. 13 (2014) 1179–1190, https://doi.org/10.4314/tjpr.v13i7.24.

[37] J.M. Barichello, M. Morishita, K. Takayama, T. Nagai, Encapsulation of hydrophilic and lipophilic drugs in PLGA nanoparticles by the nanoprecipitation method, Drug Dev. Ind. Pharm. 25 (1999) 471–476, https://doi.org/10.1081/DDC-100102197.
[38] T. Musumeci, C.A. Ventura, I. Giannone, B. Ruozi, L. Montenegro, R. Pignatello, G. Puglisi, PLA/PLGA nanoparticles for sustained release of docetaxel, Int. J. Pharm. 325 (2006) 172–179, https://doi.org/10.1016/j.ijpharm.2006.06.023.
[39] J. Yoo, Y.-Y. Won, Phenomenology of the initial burst release of drugs from PLGA microparticles, ACS Biomater. Sci. Eng. 6 (2020) 6053–6062, https://doi.org/10.1021/acsbiomaterials.0c01228.
[40] H.B. Ravivarapu, K. Burton, P.P. DeLuca, Polymer and microsphere blending to alter the release of a peptide from PLGA microspheres, Eur. J. Pharm. Biopharm. 50 (2000) 263–270, https://doi.org/10.1016/S0939-6411(00)00099-0.
[41] H. Jingbin, H. Zhang, Y. Yu, Y. Chen, D. Wang, Z. Guoqing, G. Zhou, J. Liu, Z. Sun, D. Sun, Y. Lu, Y. Zhong, Biodegradable self-assembled nanoparticles of poly (D,L-lactide-co-glycolide)/hyaluronic acid block copolymers for target delivery of docetaxel to breast cancer, Biomaterials 35 (2013), https://doi.org/10.1016/j.biomaterials.2013.09.089.
[42] M. Cózar-Bernal, M. Holgado, J. Arias, I. Muñoz, L. Martin-Banderas, J. Alvarez-Fuentes, M. Fernández-Arévalo, Insulin-loaded PLGA microparticles: flow focusing versus double emulsion/solvent evaporation, J. Microencapsul. 28 (2011) 430–441, https://doi.org/10.3109/02652048.2011.576786.
[43] C.M. Kelly, C.C. DeMerlis, D.R. Schoneker, J.F. Borzelleca, Subchronic toxicity study in rats and genotoxicity tests with polyvinyl alcohol, Food Chem. Toxicol. 41 (2003) 719–727, https://doi.org/10.1016/S0278-6915(03)00003-6.
[44] A.L. C de S L Oliveira, R.F. de Araújo Júnior, T. Gomes de Carvalho, A.B. Chan, T. Schomann, F. Tamburini, L.-F. de Geus-Oei, L.J. Cruz, Effect of oxaliplatin-loaded poly (D,L-lactide-co-glycolic acid) (PLGA) nanoparticles combined with retinoic acid and cholesterol on apoptosis, drug resistance, and metastasis factors of colorectal cancer, Pharmaceutics 12 (2020) 193, https://doi.org/10.3390/pharmaceutics12020193.
[45] M. Gaur, S. Maurya, M.S. Akhtar, A.B. Yadav, Synthesis and evaluation of BSA-loaded PLGA–chitosan composite nanoparticles for the protein-based drug delivery system, ACS Omega 8 (2023) 18751–18759, https://doi.org/10.1021/acsomega.3c00738.
[46] K.K. Chereddy, G. Vandermeulen, V. Préat, PLGA based drug delivery systems: promising carriers for wound healing activity, Wound Repair Regen. 24 (2016) 223–236, https://doi.org/10.1111/wrr.12404.
[47] L.H. Lam, T. Shimamura, S. Manabe, M. Ishiyama, H. Ukeda, Assay of angiotensin I-converting enzyme-inhibiting activity based on the detection of 3-hydroxybutyrate with water-soluble tetrazolium salt, Anal. Sci. 24 (2008) 1057–1060, https://doi.org/10.2116/analsci.24.1057.
[48] M. Hasmann, I. Schemainda, FK866, a highly specific noncompetitive inhibitor of nicotinamide phosphoribosyltransferase, represents a novel mechanism for induction of tumor cell apoptosis, Cancer Res. 63 (2003) 7436–7442.